iScience

CellPress
OPEN ACCESS

Article

Pluripotency state transition of embryonic stem cells requires the turnover of histone chaperone FACT on chromatin

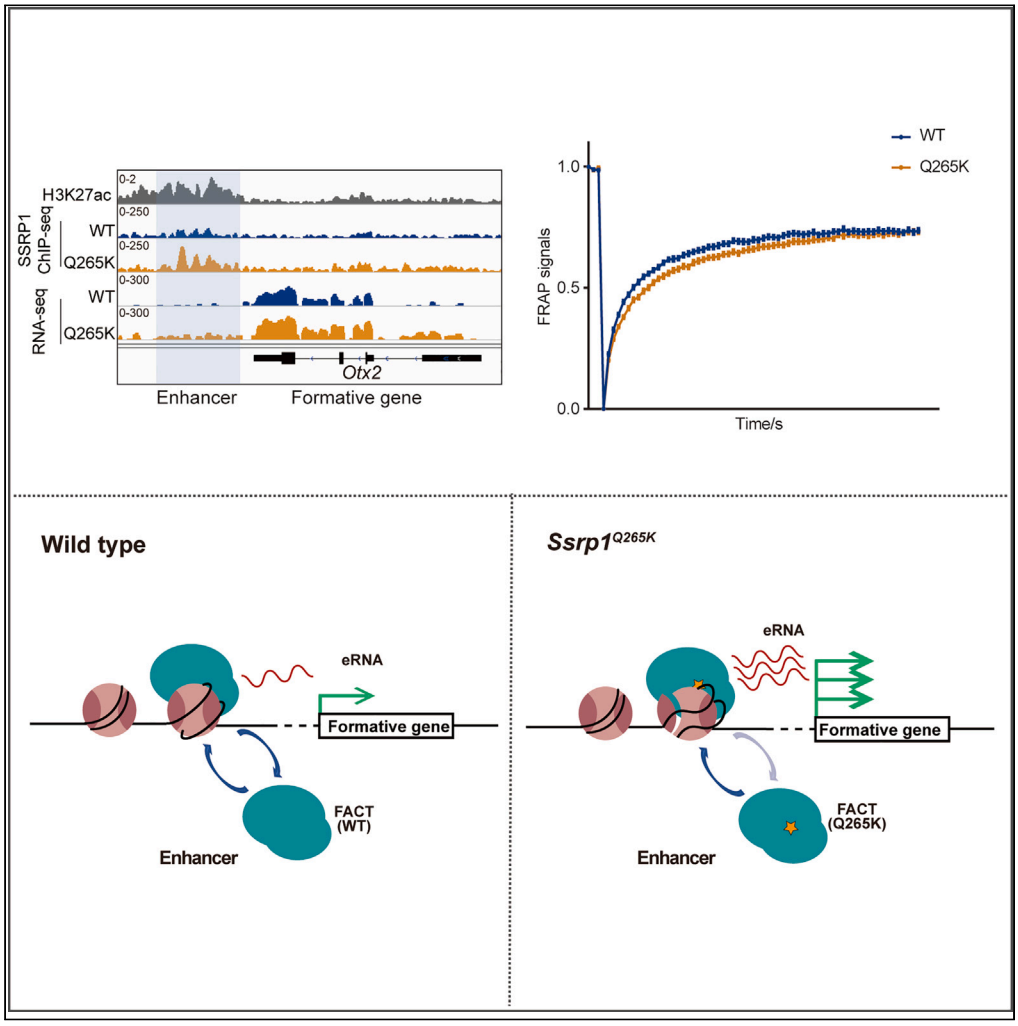

Hang Zhao, Di Li, Xue Xiao, ..., Ping Chen, Jiayi Yang, Qing Li

chenping@ccmu.edu.cn (P.C.)
yangjy2018@nim.ac.cn (J.Y.)
li.qing@pku.edu.cn (Q.L.)

Highlights

FACT$^{SSRP1\text{-}Q265K}$ increases its binding with H3-H4 and impairs nucleosome disassembly

The turnover of FACT$^{SSRP1\text{-}Q265K}$ on chromatin is impaired

FACT$^{SSRP1\text{-}Q265K}$ enhances the naive-to-formative state transition of mESCs

FACT$^{SSRP1\text{-}Q265K}$ is enriched at the enhancers of formative genes

Zhao et al., iScience 27, 108537
January 19, 2024
https://doi.org/10.1016/j.isci.2023.108537

iScience

CellPress
OPEN ACCESS

Article

Pluripotency state transition of embryonic stem cells requires the turnover of histone chaperone FACT on chromatin

Hang Zhao,[1,5] Di Li,[1,5] Xue Xiao,[4,5] Cuifang Liu,[4] Guifang Chen,[2] Xiaoyu Su,[1] Zhenxin Yan,[1] Shijia Gu,[1] Yizhou Wang,[4] Guohong Li,[4] Jianxun Feng,[1] Wei Li,[4] Ping Chen,[3,*] Jiayi Yang,[2,*] and Qing Li[1,6,*]

SUMMARY

The differentiation of embryonic stem cells (ESCs) begins with the transition from the naive to the primed state. The formative state was recently established as a critical intermediate between the two states. Here, we demonstrate the role of the histone chaperone FACT in regulating the naive-to-formative transition. We found that the Q265K mutation in the FACT subunit SSRP1 increased the binding of FACT to histone H3-H4, impaired nucleosome disassembly *in vitro*, and reduced the turnover of FACT on chromatin *in vivo*. Strikingly, mouse ESCs harboring this mutation showed elevated naive-to-formative transition. Mechanistically, the SSRP1-Q265K mutation enriched FACT at the enhancers of formative-specific genes to increase targeted gene expression. Together, these findings suggest that the turnover of FACT on chromatin is crucial for regulating the enhancers of formative-specific genes, thereby mediating the naive-to-formative transition. This study highlights the significance of FACT in fine-tuning cell fate transition during early development.

INTRODUCTION

Cell fate determination plays a fundamental role in the development of all multicellular organisms. Mouse embryonic stem cells (mESCs) are valuable tools for investigating early embryonic differentiation for its pluripotency.[1,2] These cells can be maintained in a pluripotent state in controlled culture conditions or induced to differentiate into derivatives of the three primary germ layers: ectoderm, endoderm, and mesoderm.[3,4] Pluripotency is a cellular property that allows for the orderly development of three germ layers during embryogenesis. Naive and primed are the two major states of pluripotency, and the transition between them can be induced *in vitro*.[5–7] mESCs, derived from the inner cell mass of the pre-implantation embryo, represent the naive state *in vitro*. After implantation, they mature into the primed pluripotent state, represented by epiblast-derived stem cells (EpiSCs) *in vitro*, as they share the properties of post-implantation epiblast cells.[8] The two states are distinguished by distinct morphology, polarity, chromatin states, developmental potential, and gene expression profiles.[9] An intermediate state between the naive and primed states, known as the formative state, has recently been identified.[10,11] In this stage, ESCs exit naive pluripotency to start preparing for the primed state for multi-lineage differentiation. Additionally, cells in the formative state exhibit unique chromatin states and transcriptional profiles representing an intermediate state between the naive and primed states.[12–14] However, the mechanisms underlying the transition from the naive to the formative state remain largely unexplored.

At the molecular level, transcription factor OTX2 plays a vital role in the transition from the naive to the formative state. *Otx2* expression is significantly upregulated in formative cells and is crucial for ESCs to exit from the naive pluripotency state.[15–17] Loss of the OTX2-binding site in the *Nanog* promoter affects ESCs and cell lineage specification in the pre-implantation development.[18] Besides *Otx2*, several other genes, including *Dnmt3a* and *Fgf5,* are upregulated in the formative state compared with the naive state.[14,19] The expression of these "formative-specific genes" likely promotes the exit from naive pluripotency while also controlling commitment to specific cell lineages. However, how the expression of these formative-specific genes is regulated remains elusive.

It has been shown that histone chaperones are essential for dynamic changes of chromatin during the differentiation of ESCs. For instance, histone chaperone Asf1a (anti-silencing factor 1a) helps resolve the bivalent chromatin domains, which control the lineage-specific genes in a poised state, to activate these lineage-specific genes during differentiation.[20] Another histone chaperone, CAF-1 (chromatin assembly factor 1), safeguards somatic cell identity, and depletion of CAF-1 in mouse embryonic fibroblasts (MEFs) increases cell reprogramming efficiency by

[1]State Key Laboratory of Protein and Plant Gene Research, School of Life Sciences and Peking-Tsinghua Center for Life Sciences, Peking University, Beijing 100871, China
[2]Center for Advanced Measurement Science, National Institute of Metrology, Beijing 100029, China
[3]Department of Immunology, School of Basic Medical Sciences, Capital Medical University, Beijing 100069, China
[4]National Laboratory of Biomacromolecules, CAS Center for Excellence in Biomacromolecules, Institute of Biophysics, Chinese Academy of Sciences, Beijing 100101, China
[5]These authors contributed equally
[6]Lead contact
*Correspondence: chenping@ccmu.edu.cn (P.C.), yangjy2018@nim.ac.cn (J.Y.), li.qing@pku.edu.cn (Q.L.)
https://doi.org/10.1016/j.isci.2023.108537

Yamanaka factors.[21] In mESCs, the knockdown of CAF-1 results in an increased population of 2C-like cells and compromises exit from pluripotency, likely due to defects in the formation of facultative heterochromatin at the pluripotent genes.[22] Also, the HIRA complex, which participates in the deposition of histone variant H3.3 into chromatin, has been shown to play a critical role in the transition from naive to primed pluripotency in mESCs by regulating the expression of genes involved in pluripotency and differentiation.[23] In addition, NPM1 maintains the balance between naive and primed pluripotency in mESCs by regulating the expression of genes involved in differentiation.[24] These studies imply that different histone chaperones likely function at different steps of chromatin transition during cell fate transition.

Mounting evidence suggests that histone chaperone FACT (facilitates chromatin transactions) plays a vital role in the establishment and maintenance of chromatin states in early development. FACT consists of two essential subunits, SPT16 and SSRP1 (equivalent to Pob3 in yeast) in mammalian cells.[25,26] Both subunits are highly expressed in stem cells and less in differentiated cells.[27] Depletion of SSRP1 in mESCs results in the dysregulation of developmental and pro-proliferative genes and increased proliferation of mESCs.[28] Knockout of *Supt16* (encoding SPT16) in MEFs did not affect cell viability but severely impaired their ability to execute reprogramming to the pluripotency state.[29] Intriguingly, deletion or inhibition of FACT was also reported to activate 2C-like cell-specific genes in mESC and enhance the ability of fibroblast to reprogram into iPSCs in human and nematode cells.[30,31] These results indicate that the functions of FACT must be carefully regulated to orchestrate chromatin changes during state transitions.

FACT was best-known for regulating chromatin dynamics during gene transcription, DNA replication, and DNA repair.[32–35] FACT co-purifies with RNA polymerase II (Pol II) and can bind to both nucleosomal and free histones.[32] *In vitro*, FACT has both nucleosome disassembly and assembly abilities, and it can also induce accessibility to nucleosomal DNA without ATP hydrolysis.[36,37] Structural studies have revealed that the FACT-nucleosome complex resembles a unicycle model.[38] In detail, the SPT16 dimerization domain straddles nucleosomal DNA at the dyad and forms a saddle with the SSRP1 dimerization domain. The SPT16 and SSRP1 middle domains interact with either side of the H3-H4 tetramer, constituting the unicycle wheel. The middle domain of both subunits contains two pleckstrin homology (PH) motifs.[37,39] Two pedals of the H2A-H2B dimer are docked onto tetrasomes.[40]

FACT performs at least two distinct functions during gene transcription. First, it promotes the disassembly of nucleosomes to overcome nucleosome barriers.[32,41–44] FACT disassembles H2A-H2B to facilitate RNA Pol II-mediated transcription.[33,45] Second, FACT promotes the reassembly of nucleosomes to restore chromatin structures and prevent cryptic transcription.[46–49] Single-molecule magnetic tweezer analysis reveals that in the presence of FACT, the force for nucleosome disassembly is dramatically reduced compared to the force without FACT, indicating that FACT facilitates nucleosome disassembly. Moreover, in the presence of FACT, nucleosomes can be reformed once the force is removed,[50] indicating FACT's ability for nucleosome assembly.

It is challenging to clarify FACT's function in a specific pathway, as disruption of FACT may affect various processes simultaneously. To dissect FACT's role in mESCs, we analyzed the impact of the SSRP1-Q265K mutation, equivalent to the yeast Pob3-Q308K mutation, on cell fate transition. Biochemical studies indicated that the SSRP1-Q265K mutation increases FACT's binding to H3-H4 *in vitro* and *in vivo*, properties shared with the corresponding Pob3-Q308K mutation of yeast FACT.[39,51] Single-molecule studies showed that the SSRP1-Q265K mutant compromises the nucleosome disassembly ability of FACT while having no detectable effects on nucleosome assembly. Furthermore, we found that the SSRP1-Q265K mutation results in a defect in pluripotency maintenance of mESCs and upregulation of formative-specific genes. Mechanistically, SSRP1-Q265K mutations increase the binding of FACT at the enhancers of formative-specific genes with concomitant increased expression of enhancer RNAs. Furthermore, the SSRP1-Q265K mutant FACT showed reduced turnover kinetics on chromatin. Based on these results, we propose that FACT's turnover on chromatin regulates the enhancers of formative-specific genes, thereby mediating the transition from the naive to the formative state.

RESULTS

SSRP1-Q265K mutation increases the binding of FACT with histones

Mouse FACT consists of two essential subunits, SPT16 and SSRP1 (Pob3 in yeast) (Figure 1A). It was reported that the Pob3-Q308K mutation increased the interaction of FACT with histone H3-H4 and the mutant FACT complex showed an inefficient release from the nucleosomes.[51,52] So, we introduced the equivalent Q265K mutation of SSRP1 in mESC by CRISPR-Cas9-based genomic editing to test whether the dynamic binding of FACT to chromatin is critical for cell fate transition in early development (Figure S1A). The SSRP1-Q265 residue is located in the middle domain (MD) of SSRP1 and is highly conserved among eukaryotes (Figures 1A–1C).

Two homozygous *Ssrp1*^{Q265K} mutant clones (#1 and #2 for two independent clones) were successfully obtained and verified by Sanger sequencing (Figure S1A). We first tested the effect of the Q265K mutation on the interaction between FACT and histones *in vivo* (Figures 1D and 1E). To achieve this, mESC cell lines were generated in which the C terminus of the SPT16 subunit was fused with an eGFP tag by CRISPR-Cas9 knock-in at the *Supt16* gene locus, and eGFP-tagged SPT16-containing complexes were purified from wild-type or *Ssrp1*^{Q265K} cells. The associated proteins were analyzed by Western blotting. Consistent with the observation in yeast, the amounts of histone H3 proteins associated with the FACT$^{SSRP1\text{-}Q265K}$ complex increased compared with those associated with the wild-type FACT complex (Figures 1D and 1E). Moreover, *in vitro* pull-down assay demonstrated that recombinant glutathione S-transferase (GST)-SSRP1 middle domain (GST-SSRP1-MD) fusion protein interacted with recombinant histone H3-H4, and the GST-SSRP1^{Q265K}-MD mutant protein showed increased binding (Figures 1F–1H). The increased histone binding ability was also confirmed using the recombinant FACT complex with wild-type and mutant SSRP1 (Figures S1B and S1C). Interestingly, in this *in vitro* pull-down assay using core histone octamers, we observed that the FACT$^{SSRP1\text{-}Q265K}$ complex showed much stronger binding with the histone H3, but with a slight increase in binding with H2B (Figures S1B and S1C), indicating that the SSRP1 mutation may affect the interaction between FACT with histone H3-H4 more directly.

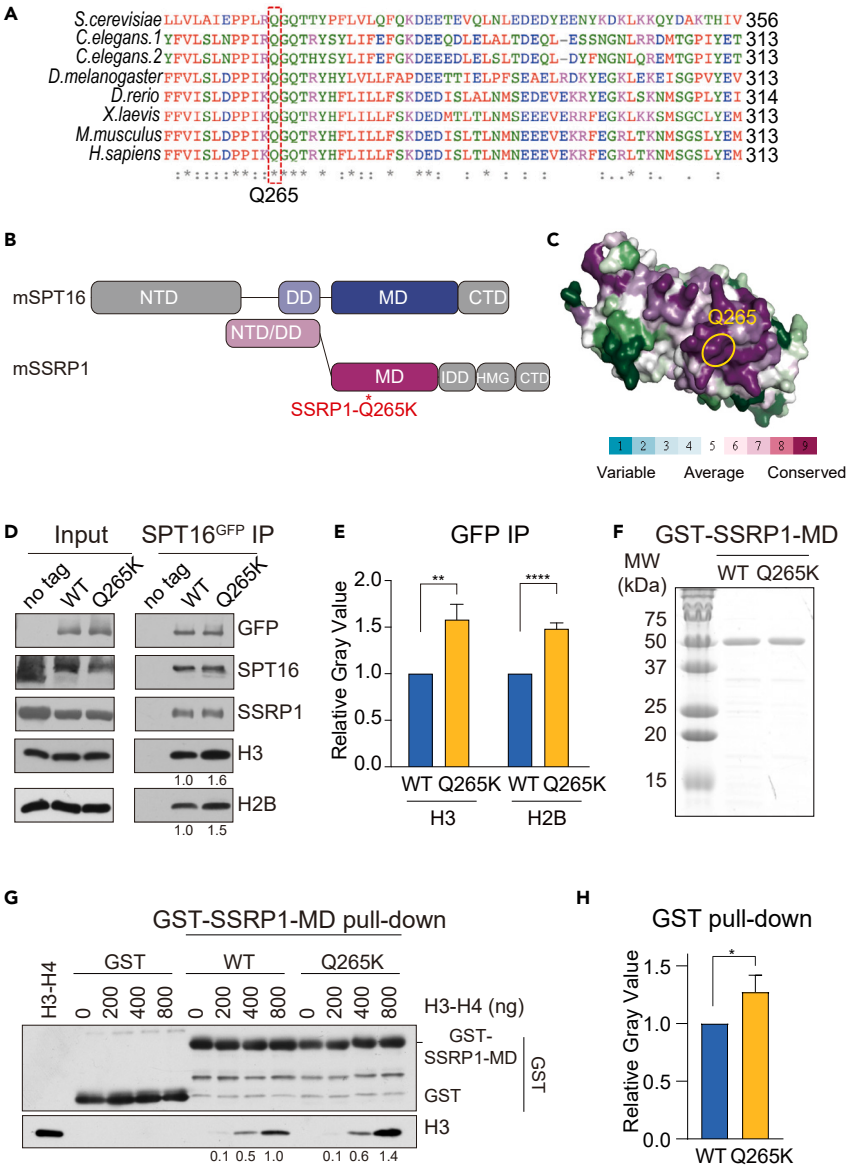

Figure 1. SSRP1-Q265K mutation increased the binding of FACT to histone H3-H4

(A) Sequence alignment of SSRP1 middle domains (MD) from seven species with the Q265 residue highlighted.

(B) Domain structure of the two FACT subunits: SPT16 and SSRP1. NTD, N-terminal domain; DD, dimerization domain; MD, middle domain; IDD, intrinsically disordered domain; HMG, HMG-box domain; CTD, C-terminal domain.

(C) Q265 is on the surface of the human SSRP1 middle domain (PDB: 4IFS). The overall conservation is color-coded.

(D) Effects of SSRP1-Q265K mutation on the ability of mutant FACT to bind histones. SPT16 and SSRP1 proteins were purified from mESCs by GFP-IP, and co-purified proteins were detected by Western blotting using indicated antibodies.

(E) Quantification of the gray levels of the Western blot bands of GFP-IP. An unpaired two-tailed Student's *t* test was performed (mean ± SD, n = 3, **p < 0.01, ****p < 0.0001).

(F) Recombinant wild-type (WT) and Q265K GST-tagged SSRP1-MD proteins were purified and detected using Coomassie brilliant blue staining (CBB).

(G) *In vitro* interaction between recombinant WT and Q265K GST-SSRP1-MD proteins with histones. WT and Q265K GST-SSRP1-MD proteins were used to pull down recombinant *Drosophila* histones H3-H4. Bound proteins were detected by Western blotting. Numbers below the panels indicate the relative H3 signal normalized to the corresponding WT sample.

(H) Quantification of the gray levels of the Western blot bands of GST pull-down. An unpaired two-tailed Student's *t* test was performed (mean ± SD, n = 3, *p < 0.05, **p < 0.01, ***p < 0.001).

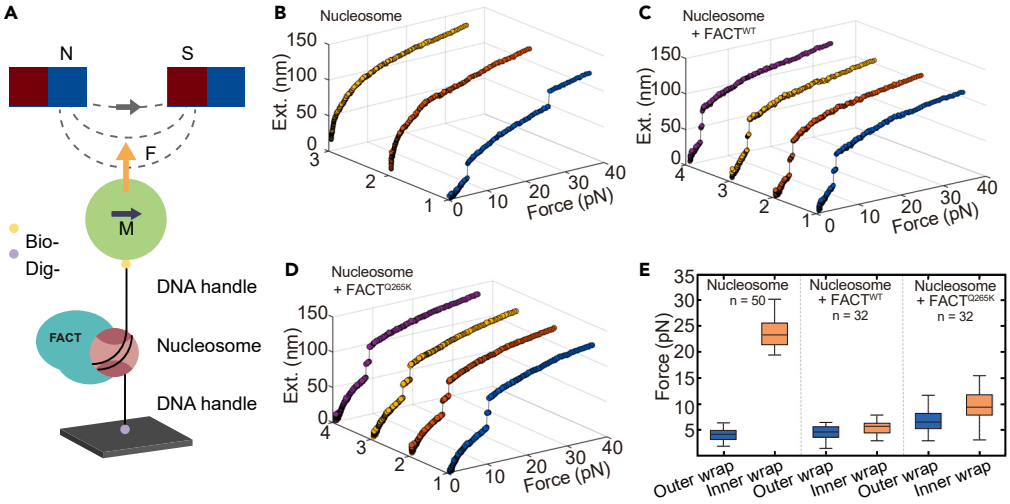

Figure 2. The FACT$^{SSRP1\text{-}Q265K}$ complex requires a more potent force to disassemble nucleosomes

(A) Schematic setup of the magnetic tweezers.

(B–D) Repeated stretching measurements of nucleosome without FACT (B), with WT FACT (C), or with FACT$^{SSRP1\text{-}Q265K}$ (D). In each stretching cycle, the force is increased at a loading rate of 0.1 pN/s. The four-color parallel lines represent repeated experiments.

(E) Statistics of rupture forces for the outer and inner DNA wraps for nucleosomes without FACT (left), with WT FACT (middle), and with FACT$^{SSRP1\text{-}Q265K}$ (right). Center lines show the median; box limits indicate the first and third quartiles. n represents the number of data values.

SSRP1-Q265K mutation impairs the destabilization effect of FACT on nucleosome *in vitro*

To analyze the impact of SSRP1-Q265K mutation on FACT's role in nucleosome dynamics, we used the single-molecule magnetic tweezer technique to trace nucleosome disassembly and assembly dynamics in the presence of wild-type or Q265K mutant FACT proteins (Figure 2A). Briefly, mono-nucleosomes were reconstituted onto a 409 bp DNA fragment with Widom 601 nucleosome positioning sequence. The two ends of DNA fragments were fixed with coverslip and paramagnetic beads. With continuously increasing tension force, the real-time trajectories of individual nucleosomes were recorded.[50] For each nucleosome in the absence of FACT, typically irreversible two-step unfolding dynamics were observed (Figure 2B), consistent well with previous results.[50] The nucleosome core particle generally contains one 147 bp DNA wrapping around the histone octamer about 1.7 rounds. Both the nucleosome assembly and disassembly can occur in a stepwise fashion, with an H3-H4 tetramer interacting with inner wrap DNA and two H2A-H2B dimers interacting with outer wrap DNA. The two extension jumps correspond well to the outer and inner DNA wrap disruptions, respectively. In the first step, the jump occurs at a lower force of about (5 $\pm$ 1.24) pN with a step size of about 21 nm, representing the unraveling of outer nucleosomal DNA wrap, which is mainly stabilized by the interaction of H2A-H2B dimer with DNA; in the second one, the jump occurs at a higher force ~(23 $\pm$ 2.82) pN with a size about 25 nm, representing to the unraveling of inner nucleosomal DNA wrap, which is mainly stabilized by the interaction of H3-H4 tetramer with DNA. When the nucleosome is totally disrupted, it cannot be reassembled correctly, as the typical two-step unfolding process of intact nucleosome cannot be observed in the following repeated stretching cycles (Figure 2B). In the presence of wild-type FACT complex, the nucleosome was disrupted entirely at a much lower tension of (5 $\pm$ 1.25) pN, which is consistent with the notion that FACT has a role in nucleosome disassembly. Meanwhile, FACT maintains the integrity of nucleosomes, evidenced by the structural transitions reversible and retaining the similar force response in each repeated stretching cycle (Figure 2C). Interestingly, the FACT$^{SSRP1\text{-}Q265K}$ complex does not affect the FACT's function to maintain the integrity of nucleosomes, but impairs the FACT's ability to facilitate nucleosome disassembly (Figure 2D): In the presence of FACT$^{SSRP1\text{-}Q265K}$, the nucleosome was totally disrupted at force ~(10 $\pm$ 3.13) pN, much higher than that of 5 pN for wild-type FACT. The statistical analysis also revealed that FACT$^{SSRP1\text{-}Q265K}$ can still destabilize the nucleosome but to a much less extent than that of wild-type FACT (Figure 2E). These results supported the idea that the SSRP1-Q265K mutation increased the interaction of FACT with nucleosomes, resulting in the retention of nucleosome stability.

Q265K FACT exhibits reduced mobility on chromatin *in vivo*

We next analyzed the mobility of FACT with wild-type or Q265K SSRP1 *in vivo* using live-cell imagining. Briefly, mESCs expressing SPT16-eGFP in wild-type and *Ssrp1*^{Q265K} background were subjected to the fluorescence recovery after photobleaching (FRAP) assay, and the mobility of SPT16-eGFP in these cells was monitored by the recovery of fluorescent signals at the bleaching spot in the nucleus. After bleaching, the averages of the relative fluorescence intensity of the bleached area were plotted to reflect SPT16-eGFP's chromatin binding dynamics. In wild-type cells, SPT16-eGFP was quickly bound to chromatin in living cells, with $T_{1/2}$ being 1.15 s after photobleaching (Figures 3A–3C). In *Ssrp1*^{Q265K} cells, it took SPT16-eGFP a longer time, with $T_{1/2}$ at 1.64 s, to recover (Figures 3A–3C). These results indicate that the SSRP1-Q265K mutant impairs the turnover of chromatin FACT, likely due in part to the increased interaction with H3-H4 proteins on chromatin.

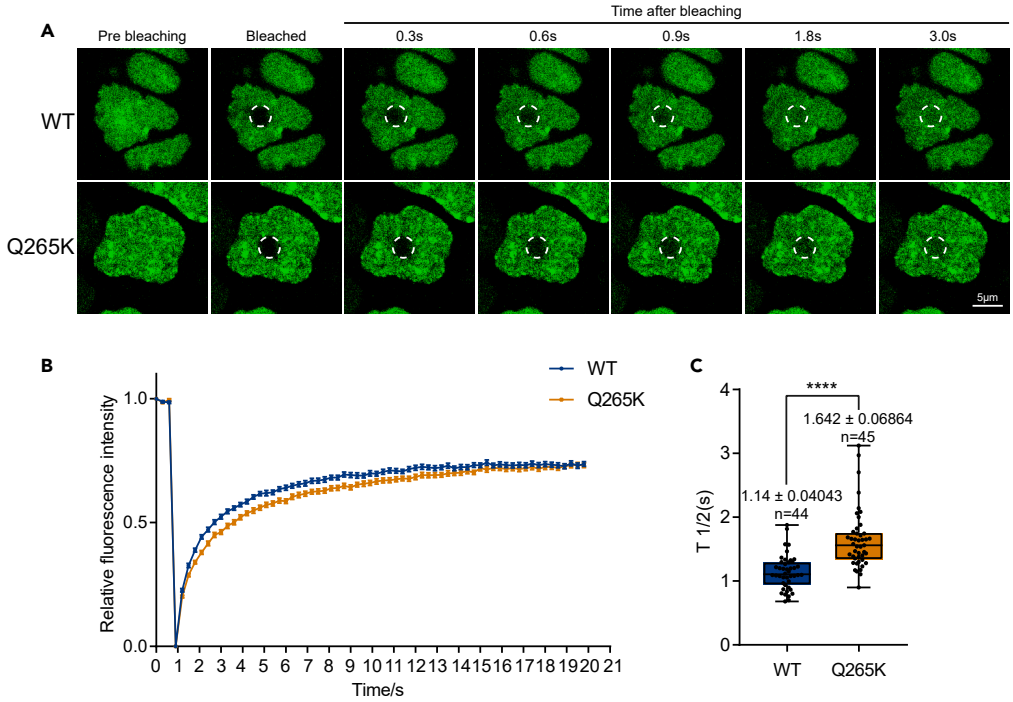

Figure 3. SSRP1-Q265K mutation reduces FACT's turnover rate on chromatin

(A) Representative images of SPT16-GFP signals in wild-type or *Ssrp1*^{Q265K} cells. The white dashed circle indicates the bleached area. Scale bar, 5μm.

(B) Quantitative analysis of relative Spt16-GFP fluorescence intensity of the bleached areas over time. The data are presented as mean ± SEM.

(C) Time for 50% fluorescence intensity recovery after photobleaching ($T_{1/2}$). Center lines show the median; box limits indicate the 1st and 3rd quartiles; the bars represent the minimum and maximum values. Each dark spot represents the individual result. The numbers above the boxplots represent the mean $T_{1/2}$ with SD. n represents the number of data values (unpaired two-tailed Student's *t* test was performed, ****$p < 0.0001$).

Ssrp1^{Q265K} cells are largely normal compared to wild-type cells in the SL2i medium

It was reported that the mouse with deletion of the *Ssrp1* gene could not survive to adulthood, and loss of SSRP1 reduces the viability of stem cells in several tissues.[53,54] We analyzed the effect of SSRP1-Q265K mutation on the growth and pluripotency of mESCs. We first cultured wild-type and *Ssrp1*^{Q265K} mESCs in the standard SL2i medium, which contains serum (S), leukemia inhibitory factor (L), and two inhibitors (2i) that inhibit GSK3β (GSKi) and MEK1/2 (MEKi), respectively. Under this culture condition, mES cells are maintained in the naive pluripotent stage.[6,55–57] We observed that both wild-type and *Ssrp1*^{Q265K} mESCs grew as round, domed-shaped colonies, which were uniform in size with clear and sharp edges (Figure S2A). In addition, alkaline phosphatase (AP) staining after a 6-day culture indicated no apparent defects in the *Ssrp1*^{Q265K} cells compared to the wild type under the SL2i culturing condition (Figures 4A and 4B). Consistent with these observations, the expression of several transcription factors such as NANOG, OCT4 (POU5F1), SOX2, and ZFP42, which are essential for maintaining pluripotency in mESCs, was similar between wild-type and *Ssrp1*^{Q265K} cells under SL2i culture conditions (Figure S2B). Furthermore, the total protein level of histone H3 and several histone modifications, including H3K4me1, H3K4me3, H3K9me3, H3K27me3, and H3K27ac that are associated with gene expression, were similar between wild-type and *Ssrp1*^{Q265K} mESCs (Figure S2C). Interestingly, although the protein levels of SPT16 and SSRP1 were decreased slightly in *Ssrp1*^{Q265K} cells compared to wild-type cells (Figure S2C), the amount of SPT16 and SSRP1 on chromatin was not altered in *Ssrp1*^{Q265K} cells compared to wild-type cells (See below, Figures 4D and S3A). This is consistent with the little change of expression profile in *Ssrp1*^{Q265K} cells under the SL2i culturing condition (Figure S2B; see below, Figure 5D).

Ssrp1^{Q265K} cells likely enter a formative-like state in the SL medium

The pluripotency of mESCs can be described in three continuum states: naive, formative, and primed. In the SL2i medium, mESCs are mainly maintained in a naive state. In contrast, when cultured in an SL medium without 2i, mESCs are a mixture of cells in naive and formative states, the latter of which represents the executive state in a developmental continuum.[58] Therefore, we tested the effects of SSRP1-Q265K mutation on changes in cell fate in the SL medium. First, similar to the SL2i condition, several key histone modifications associated with gene expression were similar between wild-type and *Ssrp1*^{Q265K} mESCs in the SL medium (Figure S3B). Interestingly, except for OCT4 (See below, Figure 5G), the expression of NANOG, SOX2, and ZFP42 was lower in the SL medium (Figure S3C).

Next, in the SL culturing condition, we found that the number of colonies in *Ssrp1*^{Q265K} cells decreased dramatically compared to wild-type cells (Figures 4A–4C). Moreover, the AP positive-stained colonies (AP^{+}) were also reduced in *Ssrp1*^{Q265K} cells compared to wild-type cells

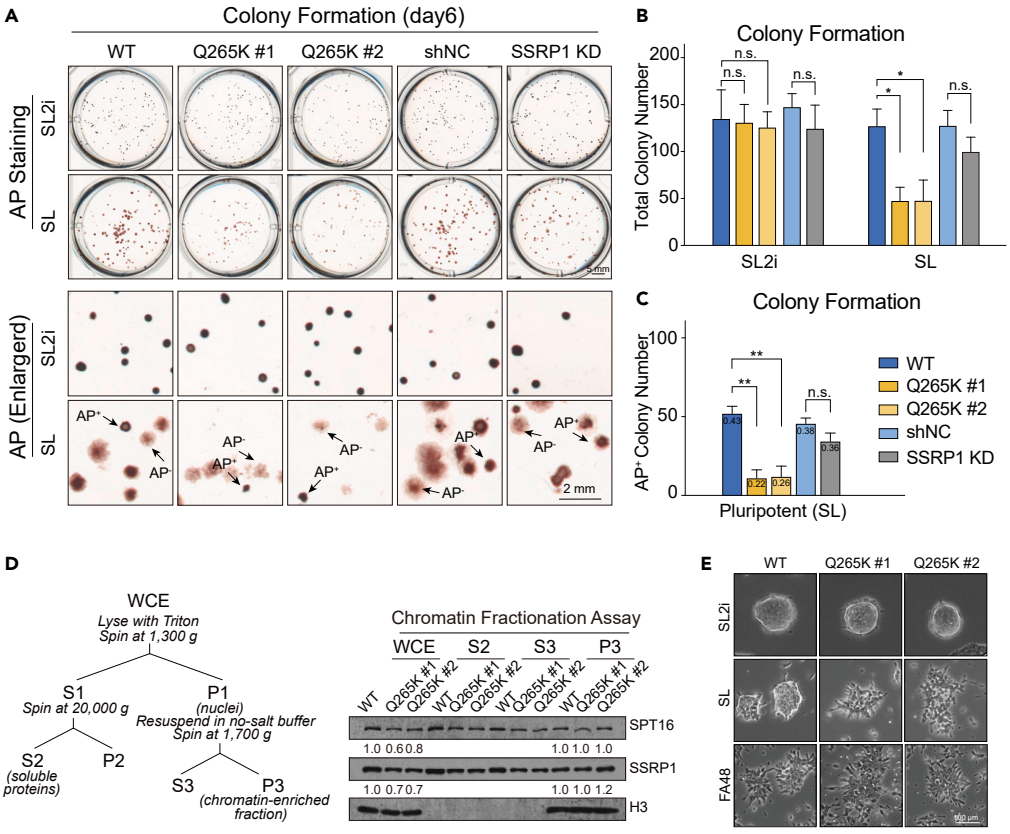

Figure 4. SSRP1-Q265K mutation leads to a defect in pluripotency maintenance of mESCs in the SL medium

(A) Representative images of AP staining of colonies six days after culturing in the SL2i and SL medium. The dark red colonies were identified as AP-positive (AP^+), as exemplified in the bottom panel. The loose light red colonies were identified as AP negative (AP^-) and were indicated by arrows. Scale bars, 5 mm and 2 mm.

(B) Quantification of colonies showed in A. The data are presented as mean ± SD (n = 3, an unpaired two-tailed Student's *t* test was performed *p < 0.05, n.s.: non-significant).

(C) Quantification of AP^+ colonies (mean ± SD, n = 3, an unpaired two-tailed Student's *t* test was performed, **p < 0.01, n.s.: non-significant). The ratio of AP^+ colonies in total colonies was labeled in the column.

(D) Analysis of chromatin binding of wild-type and Q265K FACT on chromatin using a chromatin fractionation assay. A workflow of chromatin fractionation assay in the SL medium and Western blotting of different fractions were shown. Numbers below each panel indicate the relative signal normalized to the corresponding wild-type sample.

(E) Cell morphology in the SL2i, SL medium, and FA48 condition. Scale bar, 100 μm.

(Figures 4A–4C). These results indicate that the Q265K mutation causes a defect in pluripotency maintenance in mESCs cultured in the SL medium, and the defect is likely masked by 2i when cultured in the SL2i medium. Additionally, there is no significant difference in the AP negative-stained (AP^-) cells when comparing *Ssrp1*^{Q265K} cells to wild-type cells in the SL condition (Figure S3D), raising the possibility that *Ssrp1*^{Q265K} cells are no more differentiated than wild-type cells. Finally, *Ssrp1*^{Q265K} mutant colonies showed a flattened shape different than round-shaped wild-type colonies (Figure 4E). This morphology of *Ssrp1*^{Q265K} mutant colonies resembles that of formative state cells induced by bFGF and Activin A for 48 h (FA48) (Figure 4E).[6] Therefore, *Ssrp1*^{Q265K} mESCs likely enter a state that resembles the formative state of pluripotency under the SL culturing condition.

Because the protein levels of SPT16 and SSRP1 decreased in *Ssrp1*^{Q265K} cells compared to wild-type cells (Figures S2C and S3B), we tested whether the defect in pluripotency maintenance in the SL medium was caused by reduced expression of these proteins. Therefore, we depleted SSRP1 by shRNA interfering (*Ssrp1*^{KD}) (Figure S2D), examined its impact on the formation of pluripotent colonies, and observed that depletion of SSRP1 had little effect on pluripotency maintenance in the SL medium (Figures 4A–4C, see SSRP1 KD VS shNC). This result indicates that the defect in pluripotency maintenance in *Ssrp1*^{Q265K} cells is not caused by the reduction of FACT protein levels, highlighting the importance of the utilization of *Ssrp1*^{Q265K} mutant to probe the cellular function of FACT.

SSRP1-Q265K promotes the expression of formative-specific genes in the SL medium

To understand how the *Ssrp1*^{Q265K} mutation affects the maintenance of pluripotency in the SL medium, we analyzed its impact on gene expression in the SL medium by RNA-Seq. We identified 546 differentially expressed genes (DEGs) between wild-type and *Ssrp1*^{Q265K} cells

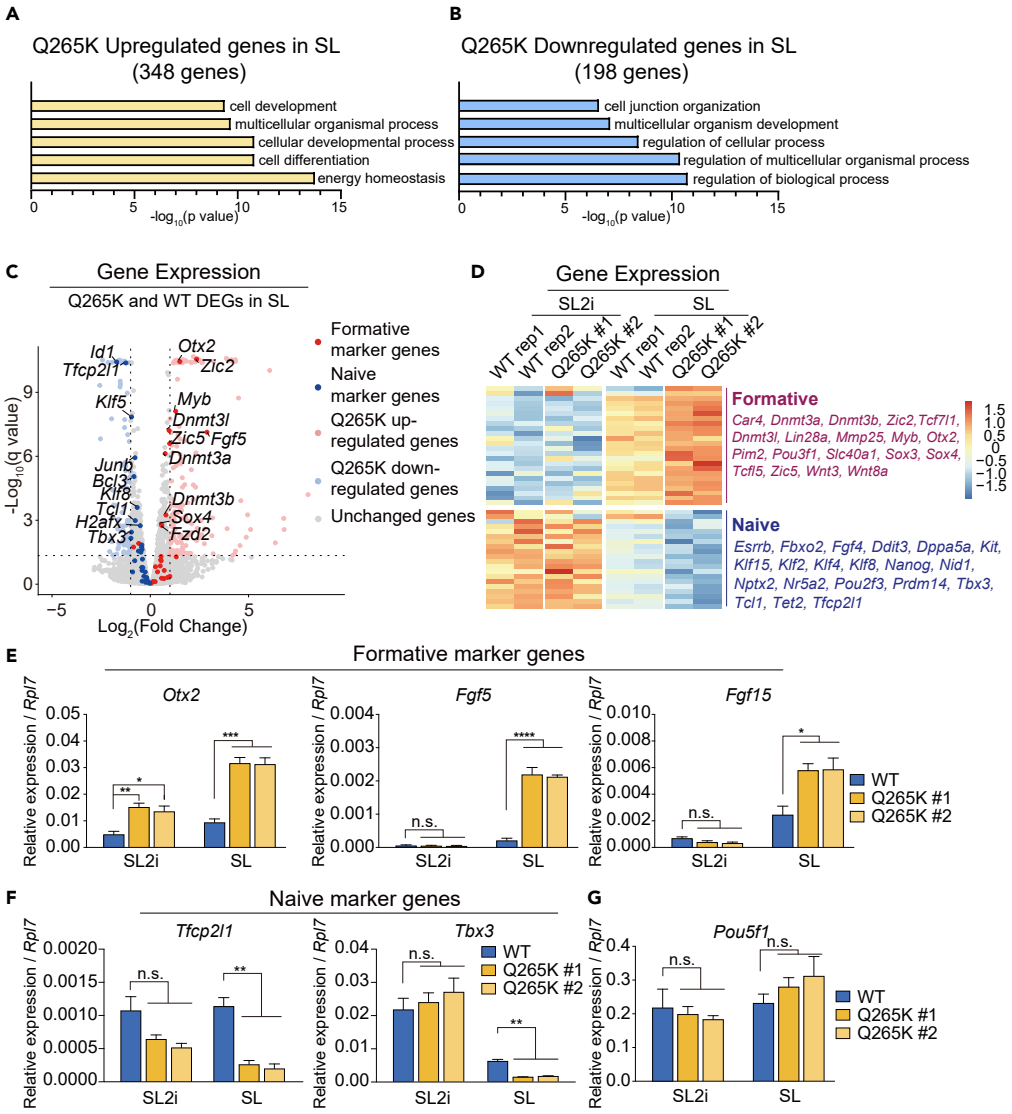

Figure 5. Effects of SSRP1-Q265K mutation on gene expression

(A and B) GO analysis of upregulated and downregulated genes in *Ssrp1*^{Q265K} cells cultured in the SL medium.

(C) Volcano plot of the DEGs under SL. Red and blue dots indicate significant changes (padj <0.05, |Log2FC| > 1).

(D) Heatmap of naive- and formative-marker genes' expression in the SL2i or SL medium. The marker genes are listed next to the heatmap.

(E–G) Marker genes' expression of WT and mutant cells measured by qPCR in the SL2i and SL medium. The level of specific gene expression was normalized to *Rpl7* (Unpaired two-tailed Student's *t* test was performed, mean ± SD, n = 3, *p < 0.05, **p < 0.01, ***p < 0.001, ****p < 0.0001, n.s.: non-significant).

with a cut-off of 2-fold change (Figure S4; Tables S1 and S2). Gene ontology analysis reveals that both the 348 upregulated and the 198 downregulated genes are enriched at various developmental processes (Figures 5A and 5B). Interestingly, many of these upregulated genes are previously known to be expressed in the formative state (Figures 5C and 5D). In contrast, many genes involved in naive state maintenance are downregulated or unchanged (Figures 5C and 5D). It was established that formative-specific genes would be upregulated and naive-specific genes would be downregulated when cells cultured in the SL2i medium were changed to the SL medium.[1] We observed similar trends in gene expression changes for both wild-type cells and *Ssrp1*^{Q265K} mutant cells between SL2i and SL conditions (Figures 5D, S5A, and S5B). However, the degree of changes is more dramatic in *Ssrp1*^{Q265K} cells than in wild-type cells (Figure 5D), consistent with the idea that a significant fraction of *Ssrp1*^{Q265K} cells is in the formative-like state in the SL medium.

By comparing our RNA-seq data with published RNA-seq data, we found that *Ssrp1*^{Q265K} cells are closer to the formative state than wild-type cells in the SL condition (Figures S6A and S6B). Besides, compared with the expression profile of the differentiated embryoid body (EB), both wild-type and *Ssrp1*^{Q265K} cells in the SL condition are likely undifferentiated (Figure S6C).

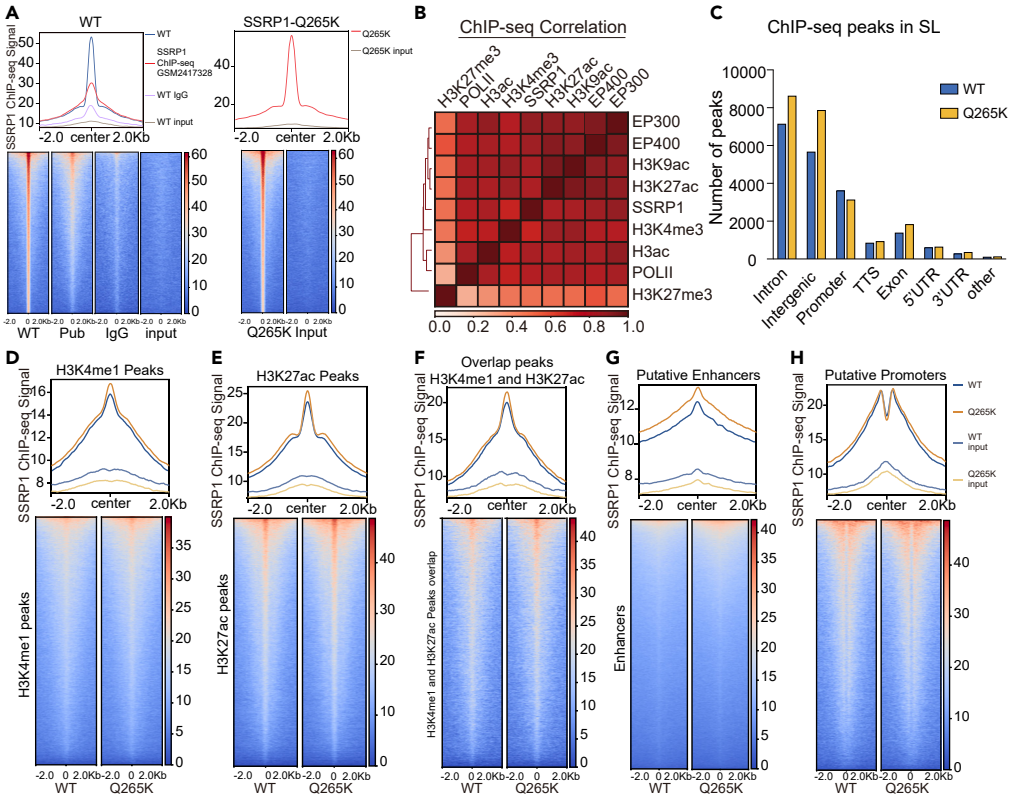

Figure 6. FACT is enriched at enhancers

(A) The average WT and Q265K SSRP1 ChIP-Seq density of two independent repeats (top) and SSRP1 ChIP-Seq signals at each peak (heatmap) were shown. ChIP-Seq using input and published SSRP1 ChIP-seq data (GEO: GSM2417328) were also shown as controls and comparisons.

(B) Correlations of ChIP-seq signals among SSRP1, Pol II (GEO: GSM1566092), H3ac (GEO: GSM2165939), H3K4me3 (GEO: GSM651193), H3K27ac (GEO: GSM1566091), H3K9ac (GEO: GSM2417092), H3K27me3 (GEO: GSM1276707), EP300 (GEO: GSM2417169), and EP400 (GEO: GSM1650013).

(C) The proportion of SSRP1 WT and Q265K ChIP-Seq peaks at the indicated genomic regions.

(D–F) SSRP1 ChIP-seq signals at peaks of H3K27ac (D), H3K4me1 (E, GEO: GSM845242), and H3K27ac and H3K4me1 (F).

(G and H) SSRP1 ChIP-seq density at putative promoters (G) and enhancers (H). The input of WT and Q265K SSRP1 were shown as controls.

To confirm the aforementioned observations, we next analyzed the expression levels of three genes expressed in the formative state (*Otx2*, *Fgf5*, and *Fgf15*) and two genes expressed in the naive state (*Tfcp2l1* and *Tbx3*) using RT-qPCR. We observed that in both wild-type and *Ssrp1*^{Q265K} cells, the expression levels of *Otx2, Fgf5,* and *Fgf15* were upregulated in SL medium compared to SL2i (Figures 5E and S4A), with a dramatic increase in expression of these three genes in *Ssrp1*^{Q265K} mutant cells compared to wild-type cells in the SL medium (Figure 5E). Interestingly, the expression of *Otx2* was higher in *Ssrp1*^{Q265K} cells than in wild-type cells even in the SL2i medium (Figure 5E). On the contrary, the expression levels of *Tfcp2l1* and *Tbx3* were downregulated in wild-type cells (Figure S4B), with a markedly more downregulation in *Ssrp1*^{Q265K} cells than in wild-type cells under the SL culture condition (Figure 5F). As a control, the *Ssrp1*^{Q265K} mutation had no apparent effect on the expression of *Pou5f1*, which was expressed in both naive and formative states (Figures 5G and S4C). These results suggest that *Ssrp1*^{Q265K} cells upregulate the expression of formative-specific genes in the SL medium, providing an explanation for their phenotypes under this condition.

SSRP1-Q265K increases FACT's enrichment at enhancers

To understand how SSRP1-Q265K mutation impacts the expression of genes specifying formative state, we analyzed the genome-wide chromatin binding of wild-type and Q265K SSRP1 using chromatin immunoprecipitation (ChIP) followed by next-generation sequencing (ChIP-Seq) under both the SL2i and the SL culturing condition. Overall, the distribution of SSRP1 on chromatin revealed by our ChIP-Seq datasets was similar to that of published datasets (Figures 6A and S7A) and the variation between the samples was measured by PCA analysis (Figure S7B). The distribution of SSRP1 on chromatin was highly correlated with marks associated with open chromatin, including RNA Pol II, active histone marks (H3K4me1/2/3 and H3K27ac), and two histone modifying enzymes (EP300 and EP400), with a low correlation with H3K27me3, a repressive mark (Figure 6B). We detected 15,811 and 18,345 SSRP1 ChIP-Seq peaks in wild-type and *Ssrp1*^{Q265K} cells, respectively. Interestingly, we found that the number of SSRP1 peaks at promoters, transcription termination sites (TTS), exons, and 5′UTR were similar between

Ssrp1^{Q265K} and wild-type cells. In contrast, the number of SSRP1 peaks at intron and intergenic regions in SL condition, which are enriched with enhancers, increases in *Ssrp1*^{Q265K} cells compared to wild-type cells (Figure 6C). On the contrary, we did not observe an apparent increase in peak numbers at these regions under the SL2i condition (Figure S7C).

Next, we compared the protein density of wild-type and Q265K SSRP1 at chromatin regions marked by specific histone modifications for active enhancers (H3K27ac and H3K4me1) and promoters (H3K4me3) under SL conditions. We found that wild-type SSRP1 signals were enriched at regions marked by H3K27ac and H3K4me1, indicating that SSRP1 is likely localized at these active enhancer regions (Figures 6D–6F). Consistent with this interpretation, SSRP1 is enriched at the putative enhancer-like sites (ELSs) (Figure 6G). Finally, SSRP1 was also enriched at the promoters (Figure 6H). Notably, the density of SSRP1-Q265K at ELS regions, including active and putative enhancers, was markedly higher than wild-type SSRP1 (Figures 6F and 6G). These results indicate that both wild-type FACT and FACT$^{SSRP1\text{-}Q265K}$ are enriched at gene regulatory elements, with FACT$^{SSRP1\text{-}Q265K}$ proteins accumulating at enhancer-like regions at a higher level than wild-type FACT.

FACT$^{SSRP1\text{-}Q265K}$ is enriched at enhancers of formative-specific genes under the SL culturing condition

To further probe FACT's role in regulating the expression of genes especially the genes involved in the formative state, we analyzed the density of wild-type and Q265K SSRP1 at the enhancers and promoters of upregulated and downregulated genes. We observed a striking enrichment of SSRP1 at the enhancers and promoters of upregulated genes in *Ssrp1*^{Q265K} cells when compared to their levels in wild-type cells (Figure S8A). Conversely, SSRP1 levels at the enhancers of downregulated genes were lower in *Ssrp1*^{Q265K} cells than in wild-type cells (Figure S8B). Moreover, our analysis revealed that Q265K SSRP1 signals in the gene body regions of upregulated group genes were moderately higher than those of wild-type SSRP1 (Figure S8C), with no discernible changes detected in the gene bodies of downregulated genes (Figure S8D). These findings strongly suggest that the elevated levels of SSRP1-Q265K at promoters and enhancers contribute to the increased expression of these genes.

Next, we analyzed the level of SSRP1 bound to promoters and enhancers of formative-specific genes and naive-specific genes. We found that the SSRP1-Q265K proteins were significantly enriched at enhancers of formative-specific genes, with a mild increase at the promoters of these genes compared to wild-type SSRP1 (Figures 7A, S8E, S8G, and S8K). The enrichment of SSRP1-Q265K protein at the enhancers of two formative genes (*Otx2* and *Dnmt3a*) was shown as an example (Figures 7B, S8I, and S8J). In contrast, wild-type and Q265K SSRP1 levels were similar at the promoters and enhancers of naive genes (Figures 7A, S8F, S8H, and S8L).

Additionally, we analyzed changes in SSRP1 ChIP-Seq signals in relation to gene expression changes when cells cultured in SL2i medium were switched to SL medium (Figure S9). In WT cells, we identified 699 upregulated genes, while in Q265K cells, there were 1930 upregulated genes (Figure S9A). Notably, 584 genes were found to overlap between the wild-type and Q265K cells, and the formative-specific genes belong to this group (Figure S9A). Furthermore, we detected 662 and 2,162 downregulated genes in wild-type and *Ssrp1*^{Q265K} cells, respectively (Figure S9B). Among these, 591 genes were overlapped between wild-type and Q265K mutant cells, with the enrichment of the naive-specific genes in this group (Figure S9B).

We then compared SSRP1 signals among different groups of genes and observed that both wild-type and Q265K SSRP1 ChIP-Seq signals at the ELS regions of upregulated genes increased upon the culture condition switch (Figures S9C and S9D). Conversely, both wild-type and Q265K SSRP1 ChIP-Seq signals at the ELS regions of downregulated genes decreased upon the culture condition switch (Figures S9C and S9D). No dramatic changes in SSRP1 signals were detected in genes that remained unchanged in these ELS regions (Figures S9C and S9D). These trends were consistent within the WT-only (Figure S9E), Q265K-only (Figure S9F), and overlapped (Figure S9G) groups of genes.

Finally, we compared SSRP1 signals at naive and formative ELS regions following the switch from SL2i to SL culture conditions. Interestingly, we observed similar trends, with SSRP1 ChIP-Seq signals at ELSs of upregulated gene groups in *Ssrp1*^{Q265K} cells increased more than those in WT cells (Figures S9H and S9I). In summary, these results demonstrate a positive correlation between SSRP1 binding and gene expression changes, including those involving naive- or formative-specific genes, under two different culturing conditions.

SSRP1-Q265K mutation results in an increased eRNA transcription at formative enhancers under the SL condition

Active enhancers can be transcribed to generate enhancer RNA (eRNA), a type of non-coding RNA that regulates the transcription of target genes through regulating chromatin structure.[59–62] To test whether the abnormal enrichment of SSRP1-Q265K in enhancer regions affects the eRNA expression, we first analyzed the RNA Pol II binding at the enhancer regions by ChIP-qPCR. We found that Pol II binding is increased at the enhancer regions of *Otx2* and *Dnmt3a* in *Ssrp1*^{Q265K} cells than in wild-type cells (Figure S10A). Next, we calculated the eRNA levels at enhancers of formative- and naive-specific genes under the SL condition. Compared to wild-type cells, the eRNA levels at enhancers of most formative specific are upregulated in *Ssrp1*^{Q265K} cells, whereas eRNAs at most enhancers of naive genes are unchanged or downregulated (Figure 7C). Increased RNA-seq reads at the enhancer regions of the *Otx2* and *Dnmt3a* genes are a clear representation of these results (Figures 7D and S10B). Together, these results indicate that abnormal accumulation of FACT$^{SSRP1\text{-}Q265K}$ on formative enhancers likely contributes to the increase of eRNA expression and upregulation of formative-specific genes.

DISCUSSION

FACT consists of two essential subunits, SPT16 and SSRP1. This study investigated the impact of the SSRP1-Q265K mutation, equivalent to the yeast Pob3-Q308K, on cell fate transition. Biochemical studies showed that the binding of FACT$^{SSRP1\text{-}Q265K}$ to H3-H4 is increased *in vivo* and *in vitro*, similar to yeast FACT with the Pob3-Q308K mutation. Single-molecule studies revealed that the SSRP1-Q265K mutation impairs the nucleosome disassembly ability of FACT while having no detectable effects on nucleosome assembly. In cells, the mutant FACT showed reduced

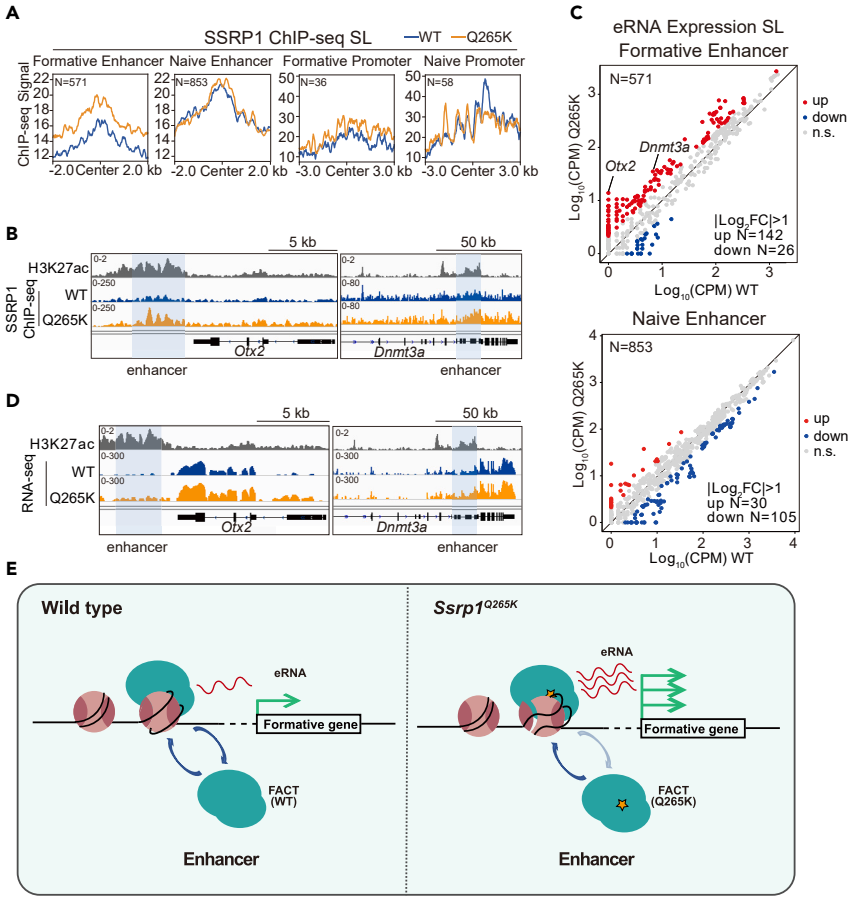

Figure 7. The association of FACT with enhancers of formative-specific genes

(A) SSRP1 ChIP-seq density at enhancers and promoters of formative- or naive-specific genes.

(B) Snapshots of IGV genome browser tracks of H3K27ac, wild-type SSRP1, and Q265K SSRP1 ChIP-seq signals at enhancers of *Otx2* and *Dnmt3a*.

(C) Scatterplots for the expression of eRNA at enhancers of formative- and naive-specific genes in WT and *Ssrp1*^{Q265K} cells cultured in the SL medium. The x-axis represents the log value of the eRNA expression in WT cells, and the y-axis represents the log value of the eRNA expression in *Ssrp1*^{Q265K} cells. Red and blue dots indicate significant changes (|Log2FC| > 1). Two independent repeats were performed.

(D) Snapshots of IGV genome browser tracks showing H3K27ac ChIP-Seq signals and RNA-seq reads at enhancers of *Otx2* and *Dnmt3a*.

(E) A model for FACT's role in regulating gene expression during mESC state transition. In response to environmental signals, FACT binds to the nucleosomes of the enhancers of certain formative-specific genes and facilitates their activation. In wild-type (WT) cells, FACT's binding is transient and detaches from these regions. In *Ssrp1*^{Q265K} cells, the interaction between FACT and nucleosomal histone H3-H4 increases, resulting in a reduced FACT turnover on chromatin and abnormal retention of FACT on these enhancer regions. Consequently, the level of eRNA expression is abnormally increased, and the formative genes are upregulated.

turnover on chromatin. Meanwhile, *Ssrp1*^{Q265K} mESCs showed defects in the maintenance of pluripotency and accumulated at the formative-like state upon removal of 2i from the medium. In addition, we found that FACT proteins were enriched at enhancer-like regions, and there is a positive correlation between SSRP1 binding at these regions and gene expression changes upon the culture condition switch. Finally, the increase in Q265K FACT binding at ELSs of upregulated genes surpasses that in WT cells, including those formative-specific genes. Based on these results, we proposed that the dynamic of FACT's turnover on chromatin is important to regulate the expression of genes involved in the transition from naive to formative state. In wild-type cells, the dynamic turnover of FACT on chromatin regulates nucleosome dynamics at the enhancers of formative-specific genes in response to environmental signals. In contrast, in *Ssrp1*^{Q265K} cells, the interaction between FACT and chromatin increases, resulting in FACT retention on chromatin. Consequently, in response to environmental signals, eRNAs at these regions and their corresponding genes are upregulated to an abnormally high level, driving cells to the formative state (Figure 7E).

A role for FACT in cell fate transition

The transition from naive to formative and then to primed pluripotency is a critical process during early embryonic development that involves extensive chromatin remodeling and changes in gene expression at each state.[12,19] This process is governed by intrinsic and extrinsic signals, which in turn regulate the proper chromatin changes essential for lineage commitment.

FACT plays significant regulatory roles in gene transcription. Previously, it was reported in budding yeast that FACT facilitates gene transcription in response to environmental stimuli.[63,64] Besides, studies from different systems/organisms have documented the role of FACT in cell fate transition/determination. For instance, it has been shown that knockout of *Supt16* in MEFs did not affect cell viability but severely impaired their ability to undergo reprogramming to the pluripotency.[29] In addition, the depletion of SSRP1 in mESCs results in a dysregulation of developmental and proliferative genes and increased cell proliferation.[28] Furthermore, FACT deficiency was shown to activate the expression of 2-cell genes in mESCs and promote fibroblast's ability to reprogram into iPSCs in human and nematode cells.[30,31] Thus, FACT is critical for both differentiation and reprogramming processes, indicating its crucial role in state transitions regardless of the direction to fulfill the need for reorganizing nucleosomes during these processes.

This study found that a mutation at the SSRP1's middle domain (Q265K) does not affect the pluripotency maintenance of mESCs at the naive state under the SL2i culturing condition. In contrast, the FACT mutant cells accumulate at formative states upon withdrawal of 2i, two inhibitors that inhibit GSK3β (GSKi) and MEK1/2 (MEKi), respectively. Furthermore, upon 2i withdrawal, formative-state specific genes (*Otx2*, *Fgf5*, and *Fgf15*) were upregulated, whereas genes involved in naive pluripotency maintenance (i.e., *Tfcp2l1* and *Tbx3*) were downregulated in mutant cells. Furthermore, our analysis revealed an enrichment of FACT proteins at enhancer-like regions, and we observed a clear positive correlation between SSRP1 binding at these regions and gene expression changes following the switch in culture conditions. Notably, the increase in Q265K FACT binding at enhancer-like regions within upregulated gene groups exceeded that seen in wild-type cells. These results strongly support that FACT regulates the expression of genes involved in the transition from naive to formative state, which plays a significant role in state transition in collaboration with extrinsic signaling pathways.

It was reported that knock-down or knock-out of *Ssrp1* changed the expression of about 3,000 or 1,100 genes in mouse ES cells.[28,30] SSRP1-Q265K mutation affected the expression of 546 genes, suggesting that the SSRP1-Q265K mutation partially compromises the function of SSRP1. Additionally, the discordance between the number of SSRP1 ChIP-Seq peaks (at least 10,000) and the number of genes whose expression is altered upon deletion of SSRP1 is reminiscent of depletion of transcription factor (TF). It is known that TFs bind thousands of sites, but the depletion of a TF affects the expression of a small number of genes.[65] Furthermore, the positive correlation between SSRP1 binding and gene expression changes, including those involving naive- or formative-specific genes, under both culturing conditions. Therefore, the reduction in SSRP1's binding could also potentially decrease the expression of these genes. However, we do not exclude the possibility that the downregulation of these genes in *Ssrp1*^{Q265K} was due to an indirect effect. For example, it is reported that overexpression of *Otx2* leads to downregulation of a group of naive-specific genes.[17] So, it is also possible that these genes' downregulation may result from the increased *Otx2* expression in *Ssrp1*^{Q265K} cells. Therefore, we suggest that FACT likely regulates the expression of genes in response to developmental cues in a context-dependent manner.

FACT turnover on chromatin is important for cell fate transition

FACT reorganizes nucleosomes during gene transcription. Previous studies on yeast FACT have established that FACT can remodel nucleosomes to increase chromatin accessibility during these DNA transactions without histone loss.[48,66,67] This remodeling activity ensures nucleosome integrity and efficient elongation of RNA Pol II during transcription.[46,68] We have shown that FACT can protect a group of nucleosomes in gene bodies to prevent divergent cryptic transcription in yeast.[48] However, it remains to be explored whether the turnover of FACT on chromatin, the ON and OFF kinetics of FACT to chromatin, is critical for the dynamic changes of gene transcription during state transition. Here we observed that SSRP1-Q265K mutation affects FACT turnover on chromatin in cells. Like yeast Pob3-Q308K mutation, we found that FACT$^{SSRP1\text{-}Q265K}$ shows an increased binding ability with histone H3-H4. A previous study showed that purified yeast FACT$^{pob3\text{-}Q308K}$ fails to release from nucleosomes efficiently,[51] indicating a reduced FACT turnover on chromatin. Consistent with this observation, our single-molecular magnetic tweezer experiments revealed that FACT$^{SSRP1\text{-}Q265K}$ requires a more potent force to disassemble nucleosomes, probably due to its increased interaction with histones. Notably, the reversibility after withdrawing force evidenced by repeated stretches is not affected by this mutation, suggesting that the ability of FACT$^{SSRP1\text{-}Q265K}$ to assemble nucleosomes is not affected. Consistently, live-cell imaging analysis using FRAP revealed a reduced exchange rate on chromatin. Together, these results indicate that FACT$^{SSRP1\text{-}Q265K}$ turnover on chromatin is reduced.

How does the reduced FACT turnover on chromatin contribute to the abnormal expression of genes involved in the transition from the naive to the formative state during cell fate control? Such a state with reduced nucleosome disassembly but maintained reassembly may lead to a less compacted nucleosome organization, resulting in a more open chromatin structure. This openness potentially facilitates easier access to DNA by transcription machineries. Consequently, gene expression may be upregulated or altered in this state. Meanwhile, the reassembly ability enables dynamic control of gene expression while preserving the overall integrity and functionality of the chromatin structure. We found that FACT is enriched at promoters, transcription start sites, and gene body regions, consistent with previous findings that SPT16 proteins are enriched at the promoter and gene bodies in yeast or fruit flies.[69–73] We also detected that FACT is enriched at active enhancers marked by H3K27ac, H3K4me1, and p300, as well as enhancers for formative-specific genes. Remarkably, the FACT$^{SSRP1\text{-}Q265K}$ ChIP-Seq signals at enhancers of formative-specific genes are higher than wild-type FACT. Retention of FACT at these enhancers is associated with increased eRNA expression and upregulation of these genes. Nonetheless, *Ssrp1*^{Q265K} cells were kept in the naive state in the SL2i condition, consistent with the idea that FACT regulates gene expression in a context-dependent manner. Thus, our results provide an impressive example of how fine-tuning the dynamics of a histone chaperone on chromatin can significantly influence nucleosome organization. This, in turn, contributes to transcriptional regulation, highlighting the significance of precise transcriptional control over gene expression in guiding cell fate decisions during early development.

Limitations of the study

This study demonstrates that the turnover of FACT proteins on chromatin significantly influences the state transition of mESCs. However, the precise factors guiding FACT to enhancers of formative-specific genes remain unclear. We hypothesize that a transcription factor may be responsible for orchestrating this process. Additionally, the mechanism by which SSRP1-Q265K impairs nucleosome disassembly is currently unknown. To gain a better understanding, it would be beneficial to examine the nucleosome's structure when bound by either wild-type or SSRP1-Q265K FACT, which could shed light on how SSRP1-Q265K enhances the interaction between FACT and histones. Finally, it's important to note that the formative state of *Ssrp1*^{Q265K} cells is transient and cannot be stably maintained under the SL condition. Future studies that allow for stable passage of formative mESCs will facilitate a more comprehensive functional profiling of formative *Ssrp1*^{Q265K} cells.

STAR★METHODS

Detailed methods are provided in the online version of this paper and include the following:

- KEY RESOURCES TABLE
- RESOURCE AVAILABILITY
  - Lead contact
  - Materials availability
  - Data and code availability
- EXPERIMENTAL MODEL AND STUDY PARTICIPANT DETAILS
  - Cell culture and reagents
- METHOD DETAILS
  - DNA extraction
  - Immunoprecipitation
  - Protein purification and *in vitro* pull-down assay
  - Flag pull-down assay
  - Western blotting
  - Fluorescence recovery after photo bleaching (FRAP)
  - FACT purification
  - Nucleosome reconstitution
  - Single-molecule magnetic tweezers analysis
  - Chromatin fractionation assay
  - Alkaline phosphatase staining
  - RNA extraction and RT-PCR analysis
  - RNA-seq and data analysis
  - Chromatin immunoprecipitation (ChIP)-sequencing (ChIP-seq) and ChIP-qPCR
  - ChIP-seq data analysis
- QUANTIFICATION AND STATISTICAL ANALYSES

SUPPLEMENTAL INFORMATION

Supplemental information can be found online at https://doi.org/10.1016/j.isci.2023.108537.

ACKNOWLEDGMENTS

We thank Dr. Yangming Wang and Dr. Peng Du (Peking University) for their generous support and helpful discussions on this project. We thank Dr. Haiyun Gan (Shenzhen Institutes of Advanced Technology) and Dr. Xiong Ji (Peking University) for their guidance on NGS data analysis. We thank Dr. Jun Ren at the National Center for Protein Sciences (Peking University) for assisting with microscopy data collection. This work was supported by the National Key Research and Development Program (2019YFA0508900 to Q.L.), the National Natural Science Foundation of China (NSFC 31725015, 31830048 to Q.L.), the Beijing Outstanding Young Scientist Program (BJJWZYJH01201910001005 to Q.L.), the National Natural Science Foundation of China (NSFC 31900433 to J.Y., 32022014 to P.C., 31991161 to G.L, 21991133 to X.X.).

AUTHOR CONTRIBUTIONS

D.L. initiated this project and conducted the mESC cell lines construction, phenotype observation, immunoprecipitation, RNA-seq, and gene expression analysis. H.Z. performed the majority of bioinformatic analysis. H.Z. and G.C. performed the FRAP experiment. H.Z. performed the *in vitro* GST pull-down analysis and Pol II ChIP analysis. J.Y. performed the SSRP1 ChIP-Seq analysis. S.G. facilitated most of the experiment preparations. X.X., C.L., Y.W., G.L., W.L., and P.C. performed the single-molecule magnetic tweezer analysis; X.S. helped with RNA-Seq data analysis; J.F. helped with data analysis and manuscript editing; Z.Y. contributed to manuscript editing; Q.L., J.Y., and P.C. supervised the project. H.Z., J.Y., D.L., and Q.L. wrote the manuscript.

DECLARATION OF INTERESTS

The authors declare no competing interests.

Received: May 30, 2023
Revised: October 6, 2023
Accepted: November 20, 2023
Published: November 28, 2023

REFERENCES

1. Endoh, M., and Niwa, H. (2022). Stepwise pluripotency transitions in mouse stem cells. EMBO Rep. *23*, e55010.
2. Hoogland, S.H.A., and Marks, H. (2021). Developments in pluripotency: a new formative state. Cell Res. *31*, 493–494.
3. Gafni, O., Weinberger, L., Mansour, A.A., Manor, Y.S., Chomsky, E., Ben-Yosef, D., Kalma, Y., Viukov, S., Maza, I., Zviran, A., et al. (2013). Derivation of novel human ground state naive pluripotent stem cells. Nature *504*, 282–286.
4. Pera, M.F., and Rossant, J. (2021). The exploration of pluripotency space: Charting cell state transitions in peri-implantation development. Cell Stem Cell *28*, 1896–1906.
5. Guo, G., Yang, J., Nichols, J., Hall, J.S., Eyres, I., Mansfield, W., and Smith, A. (2009). Klf4 reverts developmentally programmed restriction of ground state pluripotency. Development *136*, 1063–1069.
6. Hayashi, K., Ohta, H., Kurimoto, K., Aramaki, S., and Saitou, M. (2011). Reconstitution of the mouse germ cell specification pathway in culture by pluripotent stem cells. Cell *146*, 519–532.
7. Nichols, J., and Smith, A. (2009). Naive and primed pluripotent states. Cell Stem Cell *4*, 487–492.
8. Brons, I.G.M., Smithers, L.E., Trotter, M.W.B., Rugg-Gunn, P., Sun, B., Chuva de Sousa Lopes, S.M., Howlett, S.K., Clarkson, A., Ahrlund-Richter, L., Pedersen, R.A., and Vallier, L. (2007). Derivation of pluripotent epiblast stem cells from mammalian embryos. Nature *448*, 191–195.
9. Atlasi, Y., and Stunnenberg, H.G. (2017). The interplay of epigenetic marks during stem cell differentiation and development. Nat. Rev. Genet. *18*, 643–658.
10. Smith, A. (2017). Formative pluripotency: the executive phase in a developmental continuum. Development *144*, 365–373.
11. Kinoshita, M., and Smith, A. (2018). Pluripotency Deconstructed. Dev. Growth Differ. *60*, 44–52.
12. Kinoshita, M., Barber, M., Mansfield, W., Cui, Y., Spindlow, D., Stirparo, G.G., Dietmann, S., Nichols, J., and Smith, A. (2021). Capture of Mouse and Human Stem Cells with Features of Formative Pluripotency. Cell Stem Cell *28*, 453–471.e8.
13. Yu, L., Wei, Y., Sun, H.X., Mahdi, A.K., Pinzon Arteaga, C.A., Sakurai, M., Schmitz, D.A., Zheng, C., Ballard, E.D., Li, J., et al. (2021). Derivation of Intermediate Pluripotent Stem Cells Amenable to Primordial Germ Cell Specification. Cell Stem Cell *28*, 550–567.e12.
14. Wang, X., Xiang, Y., Yu, Y., Wang, R., Zhang, Y., Xu, Q., Sun, H., Zhao, Z.-A., Jiang, X., Wang, X., et al. (2021). Formative pluripotent stem cells show features of epiblast cells poised for gastrulation. Cell Res. *31*, 526–541.
15. Yang, S.H., Kalkan, T., Morissroe, C., Marks, H., Stunnenberg, H., Smith, A., and Sharrocks, A.D. (2014). Otx2 and Oct4 drive early enhancer activation during embryonic stem cell transition from naive pluripotency. Cell Rep. *7*, 1968–1981.
16. Buecker, C., Srinivasan, R., Wu, Z., Calo, E., Acampora, D., Faial, T., Simeone, A., Tan, M., Swigut, T., and Wysocka, J. (2014). Reorganization of enhancer patterns in transition from naive to primed pluripotency. Cell Stem Cell *14*, 838–853.
17. Acampora, D., Di Giovannantonio, L.G., and Simeone, A. (2013). Otx2 is an intrinsic determinant of the embryonic stem cell state and is required for transition to a stable epiblast stem cell condition. Development *140*, 43–55.
18. Acampora, D., Omodei, D., Petrosino, G., Garofalo, A., Savarese, M., Nigro, V., Di Giovannantonio, L.G., Mercadante, V., and Simeone, A. (2016). Loss of the Otx2-Binding Site in the Nanog Promoter Affects the Integrity of Embryonic Stem Cell Subtypes and Specification of Inner Cell Mass-Derived Epiblast. Cell Rep. *15*, 2651–2664.
19. Lackner, A., Sehlke, R., Garmhausen, M., Giuseppe Stirparo, G., Huth, M., Titz-Teixeira, F., van der Lelij, P., Ramesmayer, J., Thomas, H.F., Ralser, M., et al. (2021). Cooperative genetic networks drive embryonic stem cell transition from naïve to formative pluripotency. EMBO J. *40*, e105776.
20. Gao, Y., Gan, H., Lou, Z., and Zhang, Z. (2018). Asf1a resolves bivalent chromatin domains for the induction of lineage-specific genes during mouse embryonic stem cell differentiation. Proc. Natl. Acad. Sci. USA *115*, E6162–E6171.
21. Cheloufi, S., Elling, U., Hopfgartner, B., Jung, Y.L., Murn, J., Ninova, M., Hubmann, M., Badeaux, A.I., Euong Ang, C., Tenen, D., et al. (2015). The histone chaperone CAF-1 safeguards somatic cell identity. Nature *528*, 218–224.
22. Ishiuchi, T., Enriquez-Gasca, R., Mizutani, E., Bošković, A., Ziegler-Birling, C., Rodriguez-Terrones, D., Wakayama, T., Vaquerizas, J.M., and Torres-Padilla, M.-E. (2015). Early embryonic-like cells are induced by downregulating replication-dependent chromatin assembly. Nat. Struct. Mol. Biol. *22*, 662–671.
23. Zhang, M., Zhao, X., Feng, X., Hu, X., Zhao, X., Lu, W., and Lu, X. (2022). Histone chaperone HIRA complex regulates retrotransposons in embryonic stem cells. Stem Cell Res. Ther. *13*, 137.
24. Grisendi, S., Bernardi, R., Rossi, M., Cheng, K., Khandker, L., Manova, K., and Pandolfi, P.P. (2005). Role of nucleophosmin in embryonic development and tumorigenesis. Nature *437*, 147–153.
25. Reinberg, D., and Sims, R.J., 3rd (2006). de FACTo nucleosome dynamics. J. Biol. Chem. *281*, 23297–23301.
26. Wittmeyer, J., and Formosa, T. (1997). The Saccharomyces cerevisiae DNA Polymerase α Catalytic Subunit Interacts with Cdc68/Spt16 and with Pob3, a Protein Similar to an HMG1-Like Protein. Mol. Cell Biol. *17*, 4178–4190.
27. Garcia, H., Fleyshman, D., Kolesnikova, K., Safina, A., Commane, M., Paszkiewicz, G., Omelian, A., Morrison, C., and Gurova, K. (2011). Expression of FACT in mammalian tissues suggests its role in maintaining of undifferentiated state of cells. Oncotarget *2*, 783–796.
28. Mylonas, C., and Tessarz, P. (2018). Transcriptional repression by FACT is linked to regulation of chromatin accessibility at the promoter of ES cells. Life Sci. Alliance *1*, e201800085.
29. Shen, Z., Formosa, T., and Tantin, D. (2018). FACT Inhibition Blocks Induction But Not Maintenance of Pluripotency. Stem Cells Dev. *27*, 1693–1701.
30. Chen, F., Zhang, W., Xie, D., Gao, T., Dong, Z., and Lu, X. (2020). Histone chaperone FACT represses retrotransposon MERVL and MERVL-derived cryptic promoters. Nucleic Acids Res. *48*, 10211–10225.
31. Kolundzic, E., Ofenbauer, A., Bulut, S.I., Uyar, B., Baytek, G., Sommermeier, A., Seelk, S., He, M., Hirsekorn, A., Vucicevic, D., et al. (2018). FACT Sets a Barrier for Cell Fate Reprogramming in Caenorhabditis elegans and Human Cells. Dev. Cell *46*, 611–626.e12.
32. Orphanides, G., LeRoy, G., Chang, C.H., Luse, D.S., and Reinberg, D. (1998). FACT, a factor that facilitates transcript elongation through nucleosomes. Cell *92*, 105–116.
33. Belotserkovskaya, R., Oh, S., Bondarenko, V.A., Orphanides, G., Studitsky, V.M., and Reinberg, D. (2003). FACT facilitates transcription-dependent nucleosome alteration. Science *301*, 1090–1093.
34. Yang, J., Zhang, X., Feng, J., Leng, H., Li, S., Xiao, J., Liu, S., Xu, Z., Xu, J., Li, D., et al. (2016). The Histone Chaperone FACT Contributes to DNA Replication-Coupled Nucleosome Assembly. Cell Rep. *14*, 1128–1141.
35. Yarnell, A.T., Oh, S., Reinberg, D., and Lippard, S.J. (2001). Interaction of FACT, SSRP1, and the high mobility group (HMG) domain of SSRP1 with DNA damaged by the anticancer drug cisplatin. J. Biol. Chem. *276*, 25736–25741.
36. Xin, H., Takahata, S., Blanksma, M., McCullough, L., Stillman, D.J., and Formosa, T. (2009). yFACT induces global accessibility of nucleosomal DNA without H2A-H2B displacement. Mol. Cell *35*, 365–376.
37. Winkler, D.D., and Luger, K. (2011). The Histone Chaperone FACT: Structural Insights and Mechanisms for Nucleosome Reorganization. J. Biol. Chem. *286*, 18369–18374.
38. Liu, Y., Zhou, K., Zhang, N., Wei, H., Tan, Y.Z., Zhang, Z., Carragher, B., Potter, C.S., D'Arcy,

S., and Luger, K. (2020). FACT caught in the act of manipulating the nucleosome. Nature *577*, 426–431.
39. VanDemark, A.P., Blanksma, M., Ferris, E., Heroux, A., Hill, C.P., and Formosa, T. (2006). The structure of the yFACT Pob3-M domain, its interaction with the DNA replication factor RPA, and a potential role in nucleosome deposition. Mol. Cell *22*, 363–374.
40. Zhou, K., Liu, Y., and Luger, K. (2020). Histone chaperone FACT FAcilitates Chromatin Transcription: mechanistic and structural insights. Curr. Opin. Struct. Biol. *65*, 26–32.
41. Orphanides, G., Wu, W.H., Lane, W.S., Hampsey, M., and Reinberg, D. (1999). The chromatin-specific transcription elongation factor FACT comprises human SPT16 and SSRP1 proteins. Nature *400*, 284–288.
42. Orphanides, G., and Reinberg, D. (2000). RNA polymerase II elongation through chromatin. Nature *407*, 471–475.
43. Formosa, T. (2013). The role of FACT in making and breaking nucleosomes. Biochim. Biophys. Acta *1819*, 247–255.
44. Formosa, T., and Winston, F. (2020). The role of FACT in managing chromatin: disruption, assembly, or repair? Nucleic Acids Res. *48*, 11929–11941.
45. Pavri, R., Zhu, B., Li, G., Trojer, P., Mandal, S., Shilatifard, A., and Reinberg, D. (2006). Histone H2B monoubiquitination functions cooperatively with FACT to regulate elongation by RNA polymerase II. Cell *125*, 703–717.
46. Jamai, A., Puglisi, A., and Strubin, M. (2009). Histone chaperone spt16 promotes redeposition of the original h3-h4 histones evicted by elongating RNA polymerase. Mol. Cell *35*, 377–383.
47. Hainer, S.J., Pruneski, J.A., Mitchell, R.D., Monteverde, R.M., and Martens, J.A. (2011). Intergenic transcription causes repression by directing nucleosome assembly. Genes Dev. *25*, 29–40.
48. Feng, J., Gan, H., Eaton, M.L., Zhou, H., Li, S., Belsky, J.A., MacAlpine, D.M., Zhang, Z., and Li, Q. (2016). Noncoding Transcription Is a Driving Force for Nucleosome Instability in spt16 Mutant Cells. Mol. Cell Biol. *36*, 1856–1867.
49. Williams, S.K., and Tyler, J.K. (2007). Transcriptional regulation by chromatin disassembly and reassembly. Curr. Opin. Genet. Dev. *17*, 88–93.
50. Chen, P., Dong, L., Hu, M., Wang, Y.-Z., Xiao, X., Zhao, Z., Yan, J., Wang, P.-Y., Reinberg, D., Li, M., et al. (2018). Functions of FACT in Breaking the Nucleosome and Maintaining Its Integrity at the Single-Nucleosome Level. Mol. Cell *71*, 284–293.e4.
51. McCullough, L., Poe, B., Connell, Z., Xin, H., and Formosa, T. (2013). The FACT histone chaperone guides histone H4 into its nucleosomal conformation in Saccharomyces cerevisiae. Genetics *195*, 101–113.
52. Zunder, R.M., Antczak, A.J., Berger, J.M., and Rine, J. (2012). Two surfaces on the histone chaperone Rtt106 mediate histone binding, replication, and silencing. Proc. Natl. Acad. Sci. USA *109*, E144–E153.
53. Goswami, I., Sandlesh, P., Stablewski, A., Toshkov, I., Safina, A.F., Magnitov, M., Wang, J., and Gurova, K. (2022). FACT maintains nucleosomes during transcription and stem cell viability in adult mice. EMBO Rep. *23*, e53684.
54. Cao, S., Bendall, H., Hicks, G.G., Nashabi, A., Sakano, H., Shinkai, Y., Gariglio, M., Oltz, E.M., and Ruley, H.E. (2003). The high-mobility-group box protein SSRP1/T160 is essential for cell viability in day 3.5 mouse embryos. Mol. Cell Biol. *23*, 5301–5307.
55. Ying, Q.L., Wray, J., Nichols, J., Batlle-Morera, L., Doble, B., Woodgett, J., Cohen, P., and Smith, A. (2008). The ground state of embryonic stem cell self-renewal. Nature *453*, 519–523.
56. Kalkan, T., Olova, N., Roode, M., Mulas, C., Lee, H.J., Nett, I., Marks, H., Walker, R., Stunnenberg, H.G., Lilley, K.S., et al. (2017). Tracking the embryonic stem cell transition from ground state pluripotency. Development *144*, 1221–1234.
57. Mulas, C., Kalkan, T., and Smith, A. (2017). NODAL Secures Pluripotency upon Embryonic Stem Cell Progression from the Ground State. Stem Cell Rep. *9*, 77–91.
58. Kalkan, T., and Smith, A. (2014). Mapping the route from naive pluripotency to lineage specification. Philos. Trans. R. Soc. Lond. B Biol. Sci. *369*, 20130540.
59. Sawado, T., Halow, J., Bender, M.A., and Groudine, M. (2003). The beta -globin locus control region (LCR) functions primarily by enhancing the transition from transcription initiation to elongation. Genes Dev. *17*, 1009–1018.
60. Long, H.K., Prescott, S.L., and Wysocka, J. (2016). Ever-Changing Landscapes: Transcriptional Enhancers in Development and Evolution. Cell *167*, 1170–1187.
61. Arnold, P.R., Wells, A.D., and Li, X.C. (2019). Diversity and Emerging Roles of Enhancer RNA in Regulation of Gene Expression and Cell Fate. Front. Cell Dev. Biol. *7*, 377.
62. Sartorelli, V., and Lauberth, S.M. (2020). Enhancer RNAs are an important regulatory layer of the epigenome. Nat. Struct. Mol. Biol. *27*, 521–528.
63. Biswas, D., Dutta-Biswas, R., Mitra, D., Shibata, Y., Strahl, B.D., Formosa, T., and Stillman, D.J. (2006). Opposing roles for Set2 and yFACT in regulating TBP binding at promoters. Embo j *25*, 4479–4489.
64. Leng, H., Liu, S., Lei, Y., Tang, Y., Gu, S., Hu, J., Chen, S., Feng, J., and Li, Q. (2021). FACT interacts with Set3 HDAC and fine-tunes GAL1 transcription in response to environmental stimulation. Nucleic Acids Res. *49*, 5502–5519.
65. Layden, H.M., Johnson, A.E., and Hiebert, S.W. (2023). Chemical-genetics refines transcription factor regulatory circuits. Trends Cancer.
66. Erkina, T.Y., and Erkine, A. (2015). ASF1 and the SWI/SNF complex interact functionally during nucleosome displacement, while FACT is required for nucleosome reassembly at yeast heat shock gene promoters during sustained stress. Cell Stress Chaperones *20*, 355–369.
67. Myers, C.N., Berner, G.B., Holthoff, J.H., Martinez-Fonts, K., Harper, J.A., Alford, S., Taylor, M.N., and Duina, A.A. (2011). Mutant versions of the S. cerevisiae transcription elongation factor Spt16 define regions of Spt16 that functionally interact with histone H3. PLoS One *6*, e20847.
68. Cheung, V., Chua, G., Batada, N.N., Landry, C.R., Michnick, S.W., Hughes, T.R., and Winston, F. (2008). Chromatin- and Transcription-Related Factors Repress Transcription from within Coding Regions throughout the Saccharomyces cerevisiae Genome. PLoS Biol. *6*, e277.
69. Ransom, M., Williams, S.K., Dechassa, M.L., Das, C., Linger, J., Adkins, M., Liu, C., Bartholomew, B., and Tyler, J.K. (2009). FACT and the proteasome promote promoter chromatin disassembly and transcriptional initiation. J. Biol. Chem. *284*, 23461–23471.
70. Jeronimo, C., Angel, A., Nguyen, V.Q., Kim, J.M., Poitras, C., Lambert, E., Collin, P., Mellor, J., Wu, C., and Robert, F. (2021). FACT is recruited to the +1 nucleosome of transcribed genes and spreads in a Chd1-dependent manner. Mol. Cell *81*, 3542–3559.e11.
71. Takahata, S., Yu, Y., and Stillman, D.J. (2009). The E2F functional analogue SBF recruits the Rpd3(L) HDAC, via Whi5 and Stb1, and the FACT chromatin reorganizer, to yeast G1 cyclin promoters. EMBO J. *28*, 3378–3389.
72. True, J.D., Muldoon, J.J., Carver, M.N., Poorey, K., Shetty, S.J., Bekiranov, S., and Auble, D.T. (2016). The Modifier of Transcription 1 (Mot1) ATPase and Spt16 Histone Chaperone Co-regulate Transcription through Preinitiation Complex Assembly and Nucleosome Organization. J. Biol. Chem. *291*, 15307–15319.
73. Tettey, T.T., Gao, X., Shao, W., Li, H., Story, B.A., Chitsazan, A.D., Glaser, R.L., Goode, Z.H., Seidel, C.W., Conaway, R.C., et al. (2019). A Role for FACT in RNA Polymerase II Promoter-Proximal Pausing. Cell Rep. *27*, 3770–3779.e7.
74. Du, P., Pirouz, M., Choi, J., Huebner, A.J., Clement, K., Meissner, A., Hochedlinger, K., and Gregory, R.I. (2018). An Intermediate Pluripotent State Controlled by MicroRNAs Is Required for the Naive-to-Primed Stem Cell Transition. Cell Stem Cell *22*, 851–864.e5.
75. Chronis, C., Fiziev, P., Papp, B., Butz, S., Bonora, G., Sabri, S., Ernst, J., and Plath, K. (2017). Cooperative Binding of Transcription Factors Orchestrates Reprogramming. Cell *168*, 442–459.e20.
76. Chen, P.B., Chen, H.V., Acharya, D., Rando, O.J., and Fazzio, T.G. (2015). R loops regulate promoter-proximal chromatin architecture and cellular differentiation. Nat. Struct. Mol. Biol. *22*, 999–1007.
77. Bao, S., Tang, W.W., Wu, B., Kim, S., Li, J., Li, L., Kobayashi, T., Lee, C., Chen, Y., Wei, M., et al. (2018). Derivation of hypermethylated pluripotent embryonic stem cells with high potency. Cell Res. *28*, 22–34.
78. Neri, F., Rapelli, S., Krepelova, A., Incarnato, D., Parlato, C., Basile, G., Maldotti, M., Anselmi, F., and Oliviero, S. (2017). Intragenic DNA methylation prevents spurious transcription initiation. Nature *543*, 72–77.
79. Hnisz, D., Schuijers, J., Lin, C.Y., Weintraub, A.S., Abraham, B.J., Lee, T.I., Bradner, J.E., and Young, R.A. (2015). Convergence of Developmental and Oncogenic Signaling Pathways at Transcriptional Super-Enhancers. Mol. Cell *58*, 362–370.
80. Denissov, S., Hofemeister, H., Marks, H., Kranz, A., Ciotta, G., Singh, S., Anastassiadis, K., Stunnenberg, H.G., and Stewart, A.F. (2014). Mll2 is required for H3K4 trimethylation on bivalent promoters in embryonic stem cells, whereas Mll1 is redundant. Development *141*, 526–537.
81. Whyte, W.A., Bilodeau, S., Orlando, D.A., Hoke, H.A., Frampton, G.M., Foster, C.T., Cowley, S.M., and Young, R.A. (2012). Enhancer decommissioning by LSD1 during embryonic stem cell differentiation. Nature *482*, 221–225.
82. Jiang, H., Shukla, A., Wang, X., Chen, W.-y., Bernstein, B.E., and Roeder, R.G. (2011). Role for Dpy-30 in ES Cell-Fate Specification by Regulation of H3K4 Methylation within Bivalent Domains. Cell *144*, 513–525.

83. Langmead, B., and Salzberg, S.L. (2012). Fast gapped-read alignment with Bowtie 2. Nat. Methods *9*, 357–359.
84. Li, H., Handsaker, B., Wysoker, A., Fennell, T., Ruan, J., Homer, N., Marth, G., Abecasis, G., and Durbin, R.; 1000 Genome Project Data Processing Subgroup (2009). The Sequence Alignment/Map format and SAMtools. Bioinformatics *25*, 2078–2079.
85. Ramírez, F., Dündar, F., Diehl, S., Grüning, B.A., and Manke, T. (2014). deepTools: a flexible platform for exploring deep-sequencing data. Nucleic Acids Res. *42*, W187–W191.
86. Zhang, Y., Liu, T., Meyer, C.A., Eeckhoute, J., Johnson, D.S., Bernstein, B.E., Nusbaum, C., Myers, R.M., Brown, M., Li, W., and Liu, X.S. (2008). Model-based Analysis of ChIP-Seq (MACS). Genome Biol. *9*, R137.
87. Heinz, S., Benner, C., Spann, N., Bertolino, E., Lin, Y.C., Laslo, P., Cheng, J.X., Murre, C., Singh, H., and Glass, C.K. (2010). Simple Combinations of Lineage-Determining Transcription Factors Prime cis-Regulatory Elements Required for Macrophage and B Cell Identities. Mol. Cell *38*, 576–589.
88. Schindelin, J., Arganda-Carreras, I., Frise, E., Kaynig, V., Longair, M., Pietzsch, T., Preibisch, S., Rueden, C., Saalfeld, S., Schmid, B., et al. (2012). Fiji: an open-source platform for biological-image analysis. Nat. Methods *9*, 676–682.
89. Maiden, S.L., Harrison, N., Keegan, J., Cain, B., Lynch, A.M., Pettitt, J., and Hardin, J. (2013). Specific conserved C-terminal amino acids of Caenorhabditis elegans HMP-1/α-catenin modulate F-actin binding independently of vinculin. J. Biol. Chem. *288*, 5694–5706.
90. Robinson, J.T., Thorvaldsdóttir, H., Winckler, W., Guttman, M., Lander, E.S., Getz, G., and Mesirov, J.P. (2011). Integrative genomics viewer. Nat. Biotechnol. *29*, 24–26.
91. Quinlan, A.R., and Hall, I.M. (2010). BEDTools: a flexible suite of utilities for comparing genomic features. Bioinformatics *26*, 841–842.
92. Chen, T., Chen, X., Zhang, S., Zhu, J., Tang, B., Wang, A., Dong, L., Zhang, Z., Yu, C., Sun, Y., et al. (2021). The Genome Sequence Archive Family: Toward Explosive Data Growth and Diverse Data Types. Dev. Reprod. Biol. *19*, 578–583.
93. CNCB-NGDC Members and Partners (2022). Database Resources of the National Genomics Data Center, China National Center for Bioinformation in 2022. Nucleic Acids Res. *50*, D27–D38.
94. Levenstein, M.E., and Kadonaga, J.T. (2002). Biochemical analysis of chromatin containing recombinant Drosophila core histones. J. Biol. Chem. *277*, 8749–8754.
95. Wang, Y.Z., Liu, C., Zhao, J., Yu, J., Luo, A., Xiao, X., Dou, S.X., Ma, L., Wang, P.Y., Li, M., et al. (2022). H2A mono-ubiquitination differentiates FACT's functions in nucleosome assembly and disassembly. Nucleic Acids Res. *50*, 833–846.
96. Shao, X., Kang, H., Loveless, T., Lee, G.R., Seok, C., Weis, W.I., Choi, H.J., and Hardin, J. (2017). Cell-cell adhesion in metazoans relies on evolutionarily conserved features of the α-catenin·β-catenin-binding interface. J. Biol. Chem. *292*, 16477–16490.
97. Li, G., Margueron, R., Hu, G., Stokes, D., Wang, Y.H., and Reinberg, D. (2010). Highly compacted chromatin formed in vitro reflects the dynamics of transcription activation in vivo. Mol. Cell *38*, 41–53.
98. Chen, P., Zhao, J., Wang, Y., Wang, M., Long, H., Liang, D., Huang, L., Wen, Z., Li, W., Li, X., et al. (2013). H3.3 actively marks enhancers and primes gene transcription via opening higher-ordered chromatin. Genes Dev. *27*, 2109–2124.
99. Méndez, J., and Stillman, B. (2000). Chromatin association of human origin recognition complex, cdc6, and minichromosome maintenance proteins during the cell cycle: assembly of prereplication complexes in late mitosis. Mol. Cell Biol. *20*, 8602–8612.

STAR★METHODS

KEY RESOURCES TABLE

REAGENT or RESOURCE	SOURCE	IDENTIFIER
Antibodies		
Anti-GFP	ProteinTech	Cat#50430-2-AP; RRID:AB_11042881
Anti-H2B	Abcam	Cat#ab1790; RRID:AB_302612
Anti-H3	EasyBio	Cat#BE3015; RRID:AB_2941968
Anti-H3K27ac	Abcam	Cat#ab4729; RRID:AB_2118291
Anti-H3K4me1	Abcam	Cat#ab176877; RRID:AB_2637011
Anti-H3K4me3	Millipore	Cat#04-745; RRID:AB_1163444
Anti-H3K9me3	Abcam	Cat#ab8898; RRID:AB_306848
Anti-Pol II	Cell Signaling Technology	Cat#14958; RRID:AB_2687876
Anti-SPT16	Cell Signaling Technology	Cat#12191; RRID:AB_2732025
Anti-SSRP1	BioLegend	Cat#609701; RRID:AB_315731
Rabbit Control IgG	ABclonal	Cat#AC005; RRID:AB_2771930
Anti-b-ACTIN	Ruiying Biological	Cat#RLM3208; RRID: N/A
Anti-Flag	Huaxingbio	Cat#HX1819; RRID: N/A
Anti-GST	EasyBio	Cat# BE2065; RRID: N/A
Anti-b-TUBULIN	Ruiying Biological	Cat#RLM3139; RRID: N/A
Bacterial and virus strains		
Trans BL21 (DE3) Chemically Competent Cell	TransGen	CD601
Trans1-T1 Phage Resistant Chemically Competent Cell	TransGen	CD501
Chemicals, peptides, and recombinant proteins		
Benzamidine	Sigma	B6506
CHIR99021	Selleck	S1263
DPBS	Gibco	C14190500BT
DTT	Sigma	D0632
EDTA-free Protease Inhibitor Cocktail	Roche	4693132001
Ethidium bromide	Invitrogen	15585011
Fetal bovine serum	Gibco	10091-148
Gelatin	Sigma-Aldrich	G1890
GlutaMAX	Gibco	35050-061
IPTG	Ameresco	BS119
KnockOut DMEM	Gibco	10829018
LIF	Homemade	N/A
Lipo2000	Invitrogen	11668027
Non-essential amino acid	Gibco	11140-050
NP-40	Thermo	28324
Nucleoside Mix	Millipore	ES-008-D
Opti-MEM	Gibco	31985-062
PD0325901	Selleck	S1036
Penicillin/Streptomycin	Gibco	15140-122
PMSF	Sigma	P7626

(*Continued on next page*)

Continued

REAGENT or RESOURCE	SOURCE	IDENTIFIER
Proteinase K	Invitrogen	25530015
Puromycin	InvivoGen	ant-pr-1
RNase A	Invitrogen	12091021
SYBR GREEN Supermix	Bio-Rad	1725274
Triton X-100	Sigma	T8787
Trypsin-EDTA	Gibco	25200-056
Tween 20	Sigma	P1379
Critical commercial assays		
anti-Flag M2-agarose	Sigma	A2220
ChIP DNA clean & concentrator	ZYMO research	D5205
Dynabeads™ Antibody Coupling Kit	Invitrogen	14311D
Dynabeads™ MyOne™ Streptavidin C1	Invitrogen	65001
GFP Trap	ChromoTek	GTA-20
GST affinity resin	GE	17-0756-01
Protein G Sepharose 4 Fast Flow resin	Cytiva	17061801
Red-Color AP Staining Kit	SBI	AP100R-1
TransScript®One-Step gDNA Removal and cDNA Synthesis SuperMix kit	TransGen	AT311-03
Deposited data		
E5.0 RNA-seq data	Kinoshita et al.[12]	https://www.ncbi.nlm.nih.gov/geo/; accession number GSE131555
E5.5 RNA-seq data	Kinoshita et al.[12]	https://www.ncbi.nlm.nih.gov/geo/; accession number GSE131555
E6.0 RNA-seq data	Kinoshita et al.[12]	https://www.ncbi.nlm.nih.gov/geo/; accession number GSE131555
EB day10 and day13 RNA-seq data	Du et al.[74]	https://www.ncbi.nlm.nih.gov/geo/; accession number GSE112334
EP300 ChIP-seq data	Chronis et al.[75]	https://www.ncbi.nlm.nih.gov/geo/; accession number GSE90893
EP400 ChIP-seq data	Chen et al.[76]	https://www.ncbi.nlm.nih.gov/geo/; accession number GSE67580
EpiLC RNA-seq data	Bao et al.[77]	https://www.ncbi.nlm.nih.gov/geo/; accession number GSE99494
EpiSC RNA-seq data	Bao et al.[77]	https://www.ncbi.nlm.nih.gov/geo/; accession number GSE99494
ESC RNA-seq data	Kinoshita et al.[12]	https://www.ncbi.nlm.nih.gov/geo/; accession number GSE131555
Formative state cells RNA-seq data	Kinoshita et al.[12]	https://www.ncbi.nlm.nih.gov/geo/; accession number GSE131555
H3ac ChIP-seq data	Neri et al.[78]	https://www.ncbi.nlm.nih.gov/geo/; accession number GSE72853
H3K27ac ChIP-seq data	Hnisz et al.[79]	https://www.ncbi.nlm.nih.gov/geo/; accession number GSE64188
H3K27me3 ChIP-seq data	Denissov et al.[80]	https://www.ncbi.nlm.nih.gov/geo/; accession number GSE52071
H3K4me1 ChIP-seq data	Whyte et al.[81]	https://www.ncbi.nlm.nih.gov/geo/; accession number GSE27841

(*Continued on next page*)

Continued

REAGENT or RESOURCE	SOURCE	IDENTIFIER
H3K4me3 ChIP-seq data	Jiang et al.[82]	https://www.ncbi.nlm.nih.gov/geo/; accession number GSE26136
H3K9ac ChIP-seq data	Chronis et al.[75]	https://www.ncbi.nlm.nih.gov/geo/; accession number GSE90893
Pol II ChIP-seq data	Hnisz et al.[79]	https://www.ncbi.nlm.nih.gov/geo/; accession number GSE64188
SSRP1 ChIP-seq data	Mylonas et al.[28]	https://www.ncbi.nlm.nih.gov/geo/; accession number GSE90906
Experimental models: Cell lines		
V6.5 mouse embryonic stem cell	Gift from Yangming Wang Lab	N/A
Experimental models: Organisms/strains		
Ssrp1^{Q265K} mESC	This paper	N/A
Spt16^{eGFP} mESC	This paper	N/A
Ssrp1^{Q265K} *Spt16*^{eGFP} mESC	This paper	N/A
Oligonucleotides		
sgRNA for SSRP1-Q265K 5′- CACCGCGAGTTTGGCCCTGCTTGAT-3′ 5′- AAACATCAAGCAGGGCCAAACTCGC-3′	Ruibiotech	N/A
SSRP1-Q265K donor 5′- ACGAGCTCGCAGGAAGATGGTGTG GAC-3′ 5′- AATTATGCGGCCGCGGAGCAGGTAAT ACACTGG-3′	Ruibiotech	N/A
sgRNA for Spt16-GFP 5′- CACCGAGAGAAAGTAATATGAACCT-3′ 5′- AAACAGGTTCATATTACTTTCTCTC-3′	Ruibiotech	N/A
Rpl7 for qPCR 5′- CTGGCAACTTCTATGTGCCC-3′ 5′- TGCAGAACCTTACGAACCTTTG-3′	Ruibiotech	N/A
Oct4 for qPCR 5′- CAGCTCAGCCTTAAGAACAT-3′ 5′- ACTTCAGAAACATGGTCTCC-3′	Ruibiotech	N/A
Otx2 for qPCR 5′- GAATCCAGGGTGCAGGTATGG-3′ 5′- CTGAACTCACTTCCCGAGCTG-3′	Ruibiotech	N/A
Fgf5 for qPCR 5′- AGCGCGACGTTTTCTTCGT-3′ 5′- GCCATTGACTTTGCCATCCG-3′	Ruibiotech	N/A
Fgf15 for qPCR 5′- TGTTTCACCGCTCCTTCTTT-3′ 5′- TTCTCCATCCTGTCGGAATC-3′	Ruibiotech	N/A
Tbx3 for qPCR 5′- TCCGGGCTCCACTTGAAAT-3′ 5′- CCCCTACTCACACAACAATCTCAAC-3′	Ruibiotech	N/A
Tfcp2l1 for qPCR 5′- CAGCCCGAACACTACAACCAG-3′ 5′- CAGCCGGATTTCATACGACTG-3′	Ruibiotech	N/A

(*Continued on next page*)

Continued

REAGENT or RESOURCE	SOURCE	IDENTIFIER
Software and algorithms		
Trim Galore	The Babraham Institute	RRID:SCR_011847
Bowtie 2	Langmead and Salzberg.[83]	RRID:SCR_016368
SAMtools	Li et al.[84]	RRID:SCR_002105
deepTools	Ramírez et al.[85]	RRID:SCR_016366
MACS2	Zhang et al.[86]	RRID:SCR_013291
HOMER	Heinz et al.[87]	RRID:SCR_010881
Fiji	Schindelin et al.[88]	RRID:SCR_002285
FRAP Profiler	Maiden et al.[89]	N/A
GraphPad Prism	Dotmatics	RRID:SCR_002798
Integrative Genomics Viewer	Robinson et al.[90]	RRID:SCR_011793
BEDTools	Quinlan and Hall.[91]	RRID:SCR_006646

RESOURCE AVAILABILITY

Lead contact

Further information and requests for resources and reagents should be directed to and will be fulfilled by the lead contact, Qing Li (li.qing@pku.edu.cn).

Materials availability

Cell lines generated in this study are available upon request from the lead contact.

Data and code availability

- RNA-Seq and SSRP1 ChIP-Seq data has been deposited in the Genome Sequence Archive[92] in the National Genomics Data Center,[93] China National Center for Bioinformation/Beijing Institute of Genomics, Chinese Academy of Sciences (GSA: CRA009499 and CRA013178) and are publicly accessible at https://ngdc.cncb.ac.cn/gsa. Shared URL: https://ngdc.cncb.ac.cn/gsa/s/Y49mD20U.
- This paper does not report the original code.
- Any additional information required to reanalyze the data reported in this paper is available from the lead contact upon request.

EXPERIMENTAL MODEL AND STUDY PARTICIPANT DETAILS

Cell culture and reagents

Wild-type V6.5 mouse embryonic stem cells in this paper were supplied from Dr. Yangming Wang's lab at Peking University. The *Ssrp1*^{Q265K} and *Supt16*-eGFP cell lines were generated using CRISPR/Cas9-mediated homologous recombination by co-transfecting the pX459 plasmid and a donor plasmid to mESCs. The positive clones were selected with puromycin and confirmed by PCR and Sanger Sequencing.

All experiments were performed in V6.5 cells unless specified otherwise. Cells were grown in feeder-free conditions in dishes gelatinized with 0.25% gelatin (Sigma) at 37°C and 5% CO_2. Cells were cultured in KnockOut DMEM (Gibco), supplemented with 15% fetal bovine serum (Gibco), 1% nonessential amino acids (Gibco), 0.2% 2-mercaptoethanol (Gibco), 1% GlutaMAX (Gibco), 1% nucleosides (Millipore), 1% Penicillin-Streptomycin (Gibco), 30 ng/mL LIF with 1 μM PD0325901 (SelleckChem) and 3 μM CHIR99021 (SelleckChem) (SL2i) or without (SL). His-tagged LIF was purified from *E. coli*, and the plasmid was from Dr. Yangming Wang's lab (Peking University).

METHOD DETAILS

DNA extraction

1 × 10^5 cells were lysed by lysis buffer (10 mM Tris [pH 8.0], 100 mM NaCl, 10 mM EDTA, 0.5% SDS) with 2% proteinase K for 1 h at 37°C. Then, an equal volume of isopropanol was added and mixed well. After centrifuging, the precipitation was washed with 75% ethyl alcohol twice and dried at room temperature. ddH_2O was added to dissolve the genomic DNA at 55°C for 10 min. Then, the DNA can be used for PCR.

Immunoprecipitation

Cells were trypsinized and washed with DPBS. Cells were lysed in lysis buffer (50 mM HEPES-KOH [pH 7.4], 150 mM NaCl, 1 mM EDTA, 1% Triton X-100, 0.1% SDS) with protease inhibitor cocktail (Roche) on ice for 30 min. The lysate was sonicated by Bioruptor (Diagenode) for 12 cycles (10 sec ON/10 sec OFF) and centrifuged at top speed for 15 min twice. The supernatant was incubated with GFP-Trap agarose beads

(ChromoTek) for 2 h at 4°C. The beads were washed by washing buffer (50 mM HEPES-KOH [pH 7.4], 150 mM NaCl, 1 mM EDTA, 0.01% NP-40). The washed beads were mixed with 2× SDS sampling buffer and analyzed by Western blotting.

Protein purification and *in vitro* pull-down assay

GST-fused SSRP1 middle domains (WT and Q265K) were cloned to GX4T-1 plasmids and expressed in BL-21 competent *E. coli* cells by 0.1 mM isopropyl-β-D-thiogalactopyranoside (IPTG) induction at 18°C overnight. *E.coli* cells were lysed in lysis buffer (5 mM Tris-HCl [pH 8.0], 500 mM NaCl, 5% glycerol, 2 mM $MgCl_2$, 1 mM dithiothreitol (DTT), 1 mM phenylmethylsulfonyl fluoride (PMSF), 1 mM Proteinase K and bound to Glutathione Sepharose 4B beads (GE Healthcare). Beads were washed with lysis buffer, and proteins were eluted for binding assay. Recombinant *Drosophila* histone $(H3\text{-}H4)_2$ tetramers were expressed and purified from *E. coli*.[94] Briefly, freshly transformed cells were grown in LB medium containing ampicillin (100 μg/mL), and histone proteins were induced at an OD_{600} of ~0.6 by adding IPTG at a final concentration of 0.4 mM for 1 h at 37°C. The cells were collected at 4,000 rpm for 5 min and washed with 1XPBS. The pellets were resuspended in Buffer D (10 mM HEPES-KOH [pH 7.6], 1 mM EDTA, 10% glycerol, 1 mM DTT, 0.1 mM PMSF, and 2 mM Benzamidine) with 0.1 M NaCl, followed by lysing through sonication (3 cycles, 30 sec each). The lysate was then centrifuged at 10,000 rpm for 10 min, the resulted pellet was suspended in 0.25 N HCl, and dispersed with a Dounce homogenizer. The resulting suspension was next incubated at −20°C for 30 min and then centrifugated at 10,000 rpm for 10 min. The supernatant obtained was collected and neutralized with 0.125 volume of 2 M Tris base. The solution was dialyzed against Buffer D with 0.1 M NaCl, and the H3-H4 tetramers were purified by Source 15S chromatography. Peak fractions eluted at 1 M NaCl were pooled. The purified H3-H4 was extensively dialyzed against storage buffer (10 mM HEPES-KOH [pH 7.6], 1 mM DTT, 1 mM EDTA, 10 mM KCl, and 10% glycerol).

For binding assay, H3-H4 were incubated with protein in binding buffer (20 mM Tris-HCl [pH 8.0], 150 mM NaCl, 5% glycerol, and 0.1% Triton X-100) at 4°C for 4 h. Beads were washed three times with wash buffer (20 mM Tris-HCl [pH 8.0], 400 mM NaCl, 5% glycerol, and 0.1% Triton X-100), boiled for 5 min, and analyzed by Western blotting with indicated antibodies.

Flag pull-down assay

The Flag pull-down assay was performed as previously described.[95] The FACT complex was purified as described in the STAR Methods. In brief, 10 μL anti-Flag M2-agarose (Sigma) beads for each reaction were washed by PBS twice and pre-cleaned in BC300 buffer (20 mM Tris–HCl [pH 7.5], 10% glycerol, 300 mM NaCl, 0.1% NP-40, 500 μg/mL BSA) for 1 h at 4°C before FACT, H2A–H2B, and $(H3\text{-}H4)_2$ octamer were added. Then beads were washed three times with the wash buffer (20 mM Tris–HCl [pH 7.5], 10% glycerol, 300 mM NaCl, 0.5% NP-40) after overnight incubation at 4°C, 10 min each time. Finally, proteins were eluted with SDS-loading buffer and boiled, then analyzed by Western blotting.

Western blotting

Cells or protein lysates were added with SDS and boiled. Antibodies used for Western blotting were anti-SPT16 (CST 12191), anti-GFP (ProteinTech 50430-2-AP), anti-H3 (EasyBio BE3015), anti-H2B (Abcam ab1790), anti-H3K4me1 (Abcam ab176877), anti-H3K4me3 (Millipore 04-745), anti-H3K9me3 (Abcam ab8898), anti-H3K27ac (Abcam ab4729), anti-H3K27me3 (CST 9733T), anti-β-ACTIN (Ruiying Biological RLM3208), anti-β-TUBULIN (Ruiying Biological RLM3139).

Fluorescence recovery after photo bleaching (FRAP)

FRAP was performed using a Live SR spinning disk confocal microscope at 37°C with 5% CO_2 using a 100 × 1.4 oil objective. A region of interest of 4 μm^2 was chosen randomly inside a nucleus and was subjected to FRAP. Three prebleached frames were acquired, followed by bleach pulses, and recovery of fluorescence was followed for 20 s, with three frames per second. The raw data were processed by the Fiji plugin FRAP Profiler V2.[89,96]

FACT purification

Sf9 cells were infected with baculovirus containing Flag-SPT16 or His6-SSRP1 and incubated at 27°C for 72 h to purify FACT. SPT16 and SSRP1 were co-expressed for the FACT complex and were purified as previously described with minor modifications.[50] Centrifuged infected cells were resuspended in lysis buffer (20 mM Tris-HCl [pH 8.0], 150 mM NaCl, 5% glycerol, 1 mM PMSF). The recombinant FACT complex was purified in two steps. The cell extracts were first incubated with anti-Flag M2-agarose beads (Sigma) at 4°C for 8 h before being eluted in the presence of 0.5 mg/mL Flag peptide (Sigma). Second, the proteins were purified further using a Heparin HP column. The purified proteins were dialyzed and stored at −80°C in BC-100 buffer (100 mM NaCl, 10 mM Tris-HCl [pH 8.0], 0.5 mM EDTA, 20% glycerol, 1 mM DTT, 1 mM PMSF).

Nucleosome reconstitution

Recombinant histones H2A, H2B, H3, and H4 were cloned and purified as previously described.[97] In detail, recombinant human H2A, H2B, H3, and H4 were purified from *E. coli* BL21. Expressed histones were purified form the inclusion body using HiTrap SP column with AKTA FPLC (GE Healthcare) under the denaturing condition. Nucleosomes and tetrasomes were assembled using the salt-dialysis method as previously described.[98] In detail, equimolar amounts of $(H3\text{-}H4)_2$ tetramers and H2A-H2B dimers in unfolding buffer (7 M guanidinium HCl, 20 mM

Tris-HCl [pH 7.5], 10 mM DTT) were dialyzed into refolding buffer (2 M NaCl, 10 mM Tris-HCl [pH 7.5], 1 mM EDTA, 5 mM 2-mercaptoethanol), and then purified by a Superdex S200 column.The nucleosome DNA was prepared, and histone octamers/tetrasomes and DNA templates were mixed and collected as previously described.[95] For DNA preparation, a plasmid containing a single 601 sequence was amplified by PCR with a biotin (bio)-labeled forward primer [5′-(biotin) GGAAACAGCTATGACCATG] and a digoxigenin (dig)-labeled reverse primer [5′-(digoxin) GTAAAACGACGGCCAGTGAGCG]. The PCR products were subsequently loaded onto a HiTrap Q column (GE Healthcare) and eluted using a gradient ranging from 0% to 100% TE high salt buffer (10 mM Tris [pH 7.5], 1 M NaCl, 1 mM EDTA). The peak fractions were analyzed using a 5% native-PAGE gel, and the specific DNA products were subsequently pooled together. The DNA was precipitated by ethanol and resuspended in 500 μL TE buffer (10 mM Tris [pH 7.5],1 mM EDTA), then stored at −20°C. For nucleosome reconstitution, DNA and histone octamer were mixed in 2TEN buffer (10 mM Tris-HCl [pH 7.5], 1 mM EDTA, 2 M NaCl) at an equimolar ratio. The sample underwent gradient dialysis for 20 h at 4°C, with continuous dilution achieved by slowly pumping TE buffer to decrease the NaCl concentration from 2 M to 0.4 M. The reconstituted nucleosome was collected after final dialysis in TE buffer for 4 h.

Single-molecule magnetic tweezers analysis

Single-molecule magnetic tweezers analysis was performed as described before.[95] In brief, the two ends of the 409 bp DNA construct were tethered to a glass coverslip by digoxigenin and anti-digoxigenin ligation and to a 2.8 μm diameter Dynabeads (M280, Invitrogen Norway) by biotin-streptavidin ligation. Two small NdFeB magnets on the DNA constructs were controlled to pull on the Dynabeads and thus stretch the DNA molecule. A CCD camera (MC1362, Mikrotron) at 200 Hz monitored the bead's real-time position through an inverted microscope objective (UPLSAPO60XO, NA 1.35, Olympus). The extension (end-to-end distance) of the DNA construct was determined at nanometer resolution by analyzing the diffraction pattern of Dynabeads.

Chromatin fractionation assay

Chromatin fractionation assay was performed following the published method.[99] Briefly, cells were collected and resuspended (4×10^7 cells/mL) in buffer A (10 mM HEPES [pH 7.9], 10 mM KCl, 1.5 mM $MgCl_2$, 0.34 M sucrose, 10% glycerol, 1 mM DTT, proteinase inhibitors and phosphatase inhibitors). Then 0.1% Triton X-100 was added, and the cells were incubated on ice for 5 min. S1 and P1 were fractionated by centrifugation (4 min, 1,300 g, 4°C). S2 was clarified from S1 by centrifugation (15 min, 20,000 g, 4°C). P1 was lysed in buffer B (3 mM EDTA, 0.2 mM EGTA, 1 mM DTT, proteinase inhibitors and phosphatase inhibitors). P3 was fractionated by centrifugation (4 min, 1,700 g, 4°C) and resuspended in 2×SDS sample buffer.

Alkaline phosphatase staining

Alkaline phosphatase staining was performed using the Red-Color AP Staining Kit (SBI, AP100R-1) according to the manufacturer's recommendation. Briefly, 200 cells were cultured in a well of a 6-well plate for six days and incubated with AP staining solution after wash and fixation. Then, cells were washed with PBS and counted.

RNA extraction and RT-PCR analysis

Total RNA was extracted using TRIZOL (Invitrogen). cDNAs were synthesized by TransScript One-Step gDNA Removal and cDNA Synthesis SuperMix kit (TransGen) according to the manufacturer's recommendation. RT-PCR was performed using SYBR Green PCR Master Mix (BioRad). Mouse *Rpl7* was used as an internal control gene of gene expression in RT-PCR.

RNA-seq and data analysis

Total RNA was extracted the same way as RT-PCR. After rRNA was depleted, RNA-seq libraries and deep sequencing were conducted by GENEWIZ strand-specific mRNA sequencing services. Paired-end fastq files were trimmed by Trim Galore with parameters -q 20 –phred 33 –stringency 3 –length 20 -e 0.1. Trimmed fastq files were mapped to the mm10 genome by Hisat2 with default parameters. The exon-level read count was measured by featureCounts with default parameters. Different expression genes were measured by Deseq2, and the log2 fold change >1 or < −1 with adjusted p value <0.05 genes were selected for GO term analysis. GO term analysis was performed on https://go.princeton.edu. Heatmaps were generated by the CPM of the genes.

Chromatin immunoprecipitation (ChIP)-sequencing (ChIP-seq) and ChIP-qPCR

Cells were cross-linked with 1% paraformaldehyde for 10 min, quenched with 125 mM glycine for 5 min at room temperature, and washed with cold TBS twice. Fixed cells were re-suspended in cell lysis buffer (50 mM HEPES-KOH [pH 7.4], 150 mM NaCl, 1 mM EDTA, 1% Triton X-100, 0.1% SDS) and incubated on ice for 15 min. The lysates were sonicated for 25 cycles (30 sec ON/30 sec OFF) using Bioruptor (Diagenode) and then centrifuged at top speed for 10 min. The DNA content was measured by Qubit. An equal amount of chromatin was incubated with indicated antibodies (BioLegend 609701 for SSRP1, CST 14958 for Pol II) overnight on a rocker at 4°C. After binding, 30 μL Protein G beads (Cytiva) were added, and the reactions were rocked for another 3 h at 4°C. The beads were washed twice with ChIP buffer (50 mM Tris-HCl [pH 8.0], 10 mM EDTA, 100 mM NaCl, 1% Triton X-100, 0.1% sodium deoxycholate), once with high salt buffer (ChIP buffer with 500 mM NaCl), LiCl buffer (10 mM Tris-HCl [pH 8.0], 0.25 M LiCl, 0.5% NP-40, 0.5% sodium deoxycholate, 1 mM EDTA), and TE buffer. Bound chromatin was eluted and reverse-crosslinked at 65°C overnight. DNA was purified using a PCR purification kit (Qiagen) after the treatment of RNase A and

proteinase K. ChIP DNA was analyzed by real-time PCR. For ChIP-seq, 10 ng of ChIP or Input DNA were processed for library preparation by NEBNext Ultra DNA Library Prep Kit. The ChIP-seq library DNA was sequenced using Illumina Hiseq-PE150 by Novagene.

ChIP-seq data analysis

Paired-end fastq files were trimmed by Trim Galore with parameters -q 20 –phred33 –stringency 3 –length 20 -e 0.1. Trimmed fastq files were mapped to the mm10 genome by bowtie2 with default parameters. The replicated reads were removed by samtools. Bigwig files were generated using deepTools bamCoverage with parameters –binSize 100 -p 10 –normalizeUsing RPKM. Heatmaps were generated using deepTools computeMatrix (-a 2000 -b 2000 -bs 20 –skipZeros) and plotHeatmap. Peaks were called by MACS2 with parameters -g mm -p 0.001.

QUANTIFICATION AND STATISTICAL ANALYSES

Statistical analyses to determine significance were performed in Prism 8 GraphPad and are shown in figure legends, with corresponding p values. Data are presented as mean ± SEM or mean ± SD as indicated in figure legends. *$p < 0.05$, **$p < 0.01$, ***$p < 0.001$, ****$p < 0.0001$, ns, non-significant, as indicated in figure legends.

Wilcoxon test of SSRP1 ChIP-seq signal was performed in R.